Fermilab Proposal No. 542

Scientific Spokesman:
A. F. Garfinkel
Physics Department
Purdue University
W. Lafayette, IN 47907
(317) 749-2961

PROPOSAL FOR AN EXTENSION OF E(31)/(390) TO STUDY $\bar{\nu}p/\bar{\nu}n$ INTERACTIONS IN THE 15-FOOT BUBBLE CHAMBER WITH γ-CONVERTING PLATES

M. Derrick, P. Gregory, L. G. Hyman, K. Jaeger, G. Levman
R. J. Miller, B. Musgrave, P. Schreiner, R. Singer, and A. Snyder
Argonne National Laboratory

S. J. Barish, A. Engler, G. Keyes, T. Kikuchi,
R. Kraemer and J. Schlereth
Carnegie-Mellon University

V. E. Barnes, D. D. Carmony, A. F. Garfinkel, and A. T. Laasanen
Purdue University

March 25, 1977

CONTENTS

I. Summary

We request additional running for E-31 ($\bar{\nu}$p) and E-390 ($\bar{\nu}$d) with the broad-band, horn-focussed antineutrino beam to improve the statistics in our ongoing study of $\bar{\nu}$p and $\bar{\nu}$n reactions. The higher event numbers are required to elucidate the form of the weak neutral current, the origin of anomalies in antineutrino inclusive cross sections, to specify the structure of the hadronic jets resulting from $\bar{\nu}$p and $\bar{\nu}$n interactions, and to study the simple two-body strangeness-changing reactions. We request an additional 500,000 pictures, mostly with a deuterium filling of the chamber, to double our current approved data sample. We propose to insert γ-converting plates in the 15-foot bubble chamber for these exposures to enable us to detect and measure electrons and γ-rays in the final states. We will continue to make full use of the EMI.

II. Physics

Several of the interesting open questions in high energy physics can be illuminated by experiments studying antineutrino interactions with protons and neutrons. Some of the most important questions concern: (1) The structure of the neutral current (NC) interaction, both in isospin and in space-time. (2) The nature of the excess of events at high y seen in E1A data. (3) The origin of the μe events seen in several ν experiments. (4) A more detailed probing of the quark-parton model that has provided a unifying framework for the study of leptonic interactions.

The several hundred events collected from about 60,000 pictures so far taken in E-31, the only high energy $\bar{\nu}$ experiment with a simple target,

has only been sufficient to point up but not resolve these questions. We propose to increase this number of events by nearly two orders of magnitude (see Table I) by analyzing a total of 10^6 pictures, and also provide π^o and electron identification and measurement by using a series of tantalum plates in the downstream end of the chamber. Such an arrangement (Fig. 1) will allow us to better characterize the final system of particles and more accurately measure the kinematic quantities specifying the events.

The use of a deuterium filling will allow an immediate comparison of events coming from proton and neutron targets. Simple model independent tests of the NC can be made. For example, comparison of π^o with π^+ and π^- inclusive production from an isoscalar target gives an immediate test for the presence of isoscalar:isovector interference terms. However, as emphasized by Sakurai[1], the complete specification of the neutral current interaction requires measurements of νp, νn, $\bar{\nu} p$ and $\bar{\nu} n$ NC cross sections. Our experiment will provide the cross sections $d\sigma/dx$ for the NC events separately for neutrons and protons and with good statistics.

Charged-current (CC) neutrino interactions are understood in terms of the well-developed Quark Parton Model (QPM) phenomenology. The proposed experiment will check this model in several new ways. Charm particle production in νN collisions is thought to result from the valence quark transition $\nu n \rightarrow \mu^- c$, in addition to a contribution from the sea of $q\bar{q}$ pairs via $\nu \lambda \rightarrow \mu^- c$. In $\bar{\nu} N$ collisions, on the other hand, only the sea contribution should occur $\bar{\nu} \lambda \rightarrow \mu^+ \bar{c}$. Single <u>strange</u> particle production in $\bar{\nu} N$ interactions is again a valence quark transition via $\bar{\nu} p \rightarrow \mu^+ \lambda$. A comparison of strange and charm particle production in νN and $\bar{\nu} N$ collisions then may be most illuminating.

Very little data are available about either the $\Delta S = 1$ or the $\Delta C = 1$ transitions. Measurements of the strange particle production require a simple target because of the high probability for secondary interactions in a complex nucleus. Kinematic fitting can also be used to separate the single strange particle events from associated production.

The γ-converting plates will also allow us to identify final state electrons and so separate the dilepton events μ^+e^- + any, which are prime candidates for charm particle production, although other contributions are possible.

The excess of events at high y, reported by the HPW group, has been interpreted as evidence for a new heavy b quark. The proposed experiment will collect some thousands of such high y events, allowing their characteristics to be studied. Simple tests like the presence or absence of strangeness and high transverse momentum can be done immediately. The whole event sample can be used to refine our understanding of the QP model. For example, a comparison of the high x behavior of $\bar{\nu}p$ compared to $\bar{\nu}n$ events measures the leading quark momentum distribution in the nucleon. Detailed measurements of the jet structure, resulting from quark fragmentation, can be made using the π^o as well as charged pions. For the associated production and single strange particle events, the location of the strangeness in the jet will provide further tests of the model.

These and other physics topics are discussed in detail in the remainder of the proposal. There is clearly a wealth of physics that will result from a high statistics study of $\bar{\nu}p$ and $\bar{\nu}n$ interactions. The combination of the horn-focussed beam and the 15-foot bubble chamber provides an excellent technique for doing such experiments, and the addition of downstream metal plates

will significantly enhance the experiment.

II-A. Structure of the Weak Neutral Current

Although existing neutral current data agrees with the Weinberg model, a direct determination of the space-time and isospin structure of the weak neutral current remains a crucial experimental problem.

1. R Measurements

Studies of inclusive neutral current interactions have been reported[2] by the two electronic neutrino experiments at FNAL. Since such interactions contain an undetectable final state neutrino, even the measurement of the ratio of neutral current to charged-current total cross section R is a difficult experimental task. After eliminating or correcting for neutron induced background, one must calculate the number of real charged current events assigned to the neutral current; events called charged-current or lost entirely by imposition of a visible energy requirement must also be estimated. This requires extensive Monte Carlo studies which must make assumptions not only about the form of the weak interactions, but about the properties of the final state hadronic system. We have made a first measurement of $R^{\bar{\nu}p}$ with a sample of 127 neutral current candidates from the runs of E31.[3] Having a mixture of $\bar{\nu}$ and ν events, we measure the following relation:

$$R^{\bar{\nu}p} = 0.54 - 0.3\, R^{\nu p} \quad .$$

Fig. 2 shows the limits this places on $\sin^2\theta_w$. Thus, for example, if we assume $R^{\nu p} = 0.3$, we obtain $R^{\bar{\nu}p} = 0.45 \pm 0.12$.

The basic separation of events into the neutral current and charged current channels will be aided both by EMI improvements and by the use of the gamma detecting plates. Since the plates substantially improve the

measurement of the vector momentum of the hadronic system, one can require for CC events that its transverse component be balanced by a μ^+. In addition, our systematic uncertainty would be much reduced if we had gamma converting plates in the chamber to allow us to include the energy of π^o's when making our visible energy cut.

2. Model Dependent Analysis of Inclusive Neutral Current Reactions

In a recent paper[4] Hung and Sakurai write the effective Lagrangian for neutral current interactions (assumed to contain only vector and axial vector terms)

$$\mathcal{L} = -(G/\sqrt{2})\ \bar{\nu}\gamma_\lambda\ (1+\gamma_5)\nu\ \{\tfrac{1}{2}[\bar{u}\gamma_\lambda\ (\alpha+\beta\gamma_5)u - \bar{d}\gamma_\lambda\ (\alpha+\beta\gamma_5)d]$$
$$+\tfrac{1}{2}[\bar{u}\gamma_\lambda\ (\gamma+\delta\gamma_5)u + \bar{d}\gamma_\lambda\ (\gamma+\delta\gamma_5)d] + \bar{s}\gamma_\lambda\ (\gamma'+\delta'\gamma_5)s$$
$$+ \text{possible } c\bar{c},\ t\bar{t},\ \text{and } b\bar{b} \text{ terms}\} \ .$$

Using this quark model Lagrangian, they derive the following relations:

$$\frac{(d\sigma^{\nu p}_{NC} + d\sigma^{\nu n}_{NC}) + (d\sigma^{\bar{\nu} p}_{NC} + d\sigma^{\bar{\nu} n}_{NC})}{(d\sigma^{\nu p}_{CC} + d\sigma^{\nu n}_{CC}) - (d\sigma^{\bar{\nu} p}_{CC} + d\sigma^{\bar{\nu} n}_{CC})} = \frac{1}{4}(\alpha^2+\beta^2+\gamma^2+\delta^2)$$

$$\frac{(d\sigma^{\nu p}_{NC} + d\sigma^{\nu n}_{NC}) - (d\sigma^{\bar{\nu} p}_{NC} + d\sigma^{\bar{\nu} n}_{NC})}{(d\sigma^{\nu p}_{CC} + d\sigma^{\nu n}_{CC}) - (d\sigma^{\bar{\nu} p}_{CC} + d\sigma^{\bar{\nu} n}_{CC})} = \frac{1}{2}(\alpha\beta+\gamma\delta)$$

$$\frac{(d\sigma^{\nu p}_{NC} + d\sigma^{\bar{\nu} p}_{NC}) - (d\sigma^{\nu n}_{NC} + d\sigma^{\bar{\nu} n}_{NC})}{(d\sigma^{\nu p}_{CC} + d\sigma^{\bar{\nu} n}_{CC}) - (d\sigma^{\nu n}_{CC} + d\sigma^{\bar{\nu} p}_{CC})} = -\frac{1}{2}(\alpha\gamma+\beta\delta)$$

$$\frac{(d\sigma^{\nu p}_{NC} - d\sigma^{\bar{\nu} p}_{NC}) - (d\sigma^{\nu n}_{NC} - d\sigma^{\bar{\nu} n}_{NC})}{(d\sigma^{\nu p}_{CC} - d\sigma^{\bar{\nu} n}_{CC}) - (d\sigma^{\nu n}_{CC} - d\sigma^{\bar{\nu} p}_{CC})} = -\frac{1}{2}(\alpha\delta+\beta\gamma)$$

where $d\sigma$ may stand for $d\sigma/dxdy$ or $d\sigma/dx$. These first two ratios depend on the sum of cross sections for neutrons and protons and hence can be studied

in an isoscalar nucleus. The second set is only measured on a deuteron target, where the proton and neutron events can be separated.

The measurement of these differential cross sections is technically rather difficult even with a fine-grained detector. Using the gamma-converting plates, we will be able to measure $x \equiv (Q^2/2M\nu)$ rather well for those events in which we identify and measure the final state nucleon. These events correspond to about 30% of the neutral current sample or 2000 events, and Fig. 3 shows the estimated uncertainty in the x values for this sample.

However, y is difficult to determine even if one measures the momentum of the final state nucleon. The variable y is defined as the ratio of the final state hadron energy E_H to the incident neutrino energy E_ν. E_H can be measured reasonably well as shown in Fig. 4. However, E_ν depends not only on measurement of E_H, but on P_H, the momentum of the hadronic system, and $\cos\theta_H$, the cosine of the angle between the hadronic system and the beam direction through

$$E_\nu = \frac{M_H^2 + M_p^2 - 2M_p E_H}{2(E_H - P_H \cos\theta_H - M_p)} \quad .$$

Although P_H and $\cos\theta_H$ are reasonably well measured, see Figs. 5 and 6, the fact that $\cos\theta_H \approx 1$ means that the uncertainties in E_H and P_H are highly magnified in uncertainties in E_ν (Figs. 7 and 8).

Fig. 9 from Hung and Sakurai shows the sensitivity of the ratio $\frac{d\sigma}{dx}^{\bar{\nu}n} / \frac{d\sigma}{dx}^{\bar{\nu}p}$ to various assumed forms of the interaction. This measurement can probably only be made in a deuterium bubble chamber. To determine the constants a through δ, we propose to compare our results with those of the corresponding neutrino experiment. Final ambiguities are resolvable (in principle) by studying the diffractive reactions:

$$\bar{\nu} + N \rightarrow \bar{\nu} + \rho^{o}(\omega, \phi) + N$$

and

$$\bar{\nu} + N \rightarrow \bar{\nu} + A_1^0 + N \quad ,$$

which only the bubble chamber can hope to accomplish. The rates, however, are probably very low.

3. Model Independent Analysis of Inclusive Neutral Current Reactions

Wolfenstein and Wyler have recently[5] discussed procedures for determining the coupling constants of the Weak Neutral Current in a model-independent way. They also discuss simple tests to qualitatively determine its isospin structure. They write the hadronic neutral current N_λ as

$$N_\lambda = \frac{1}{2} g_V (\bar{u}\gamma_\lambda u - \bar{d}\gamma_\lambda d) + \frac{1}{2} g_A (\bar{u}\gamma_\lambda \gamma_5 u - \bar{d}\gamma_\lambda \gamma_5 d)$$
$$+ g'_V V^o_\lambda + g'_A A^o_\lambda \quad ,$$

where the isoscalar currents V^o_λ and A^o_λ are assumed not to include strangeness or charm. They determine the various coupling constants in terms of the cross sections σ for the inclusive reaction

$$\nu(\bar{\nu}) + N \rightarrow \nu(\bar{\nu}) + X$$
$$\nu(\bar{\nu}) + N \rightarrow \mu^-(\mu^+) + X$$

and the following tensor components in isospin space

$$T_1 \equiv \langle N(\pi^+) \rangle - \langle N(\pi^-) \rangle$$
$$T_2 \equiv \langle N(\pi^+) \rangle + \langle N(\pi^-) \rangle - 2\langle N(\pi^o) \rangle$$
$$T_0 \equiv \langle N(\pi^+) \rangle + \langle N(\pi^-) \rangle + \langle N(\pi^o) \rangle \quad .$$

Qualitatively, for either $\bar{\nu}p$ or $\bar{\nu}d$ reactions, a nonzero value of T_2 implies the existence of an isovector current. Measuring T_2 requires the γ plates for π^o detection. A simpler test can be made in $\bar{\nu}d$ reactions (isoscalar target) where a nonzero value of σT_1 implies the existence of both isoscalar and isovector currents.

Actual coupling constant determinations in this scheme depend on comparing the tensors for both neutrino and antineutrino interactions. For example, the isovector couplings g_A and g_V enter into relations of the following type:

$$\frac{\sigma T_2(\nu, \nu, d) - \sigma T_2(\bar{\nu}, \bar{\nu}, d)}{\sigma T_2(\nu, \mu^-, d) - \sigma T_2(\bar{\nu}, \mu^+, d)} = -\frac{g_V g_A}{\cos^2\theta_c}$$

where the arguments of T_2 are the identities of the incident lepton, the final lepton, and the target, respectively.

The beauty of this method is that one is allowed to make kinematic selection of the final states in such a way as to have good acceptance and particle identification so long as one does so in a charge-independent way. While the isospin tests would be done with data from this experiment alone, the detailed determination of the coupling constants would come from a comparison of our data with corresponding neutrino data.

4. Antineutrino-Electron Elastic Scattering ($\bar{\nu}_\mu e^- \rightarrow \bar{\nu}_\mu e^-$)

Antineutrino-electron elastic scattering, in particular $\bar{\nu}_\mu e^- \rightarrow \bar{\nu}_\mu e^-$, is a fundamental reaction in the study of neutral currents. The cross section is, of course, very small. Its minimum value (in the Weinberg model), corresponding to $\sin^2\theta_w = 0.125$, is $\sigma_{min} = \frac{G^2 m_e}{8\pi} E_{\bar{\nu}}(\text{GeV}) = 1.42 \times 10^{-42} E_{\bar{\nu}}$ cm^2/electron. Using the favored[6] Weinberg angle of $\sin^2\theta_w = 0.35$ leads to an approximate doubling of that cross section and an expectation of observing eight events in the proposed experiment. Fig. 10 shows the dependence of the cross section on $\sin^2\theta_w$.

The cross section is small and so the detection of this reaction has been beset by severe background problems from things like asymmetric electron-positron pairs from γ conversion, Compton electrons, and the reaction

$\nu_e n \rightarrow e^- p$. The background situation in a hydrogen/deuterium bubble chamber with downstream plates is ideal. This is because it is a separated function detector with the hydrogen serving as the target and the plates serving as the electron detector. This allows the neutrino interaction point to be studied in detail, without giving up excellent electron detection efficiency, and so permits a strong rejection of asymmetric electron-positron pairs.

The technical difficulties of the experiment can be seen from comparing the results of two CERN experiments. The heavy liquid bubble chamber group[7] (based on three events) obtained $\sigma(\bar{\nu}_\mu e \rightarrow \bar{\nu}_\mu e) = 1.0 \,^{+\,2.1}_{-\,0.9} \times 10^{-42} E_{\bar{\nu}}$ (GeV) cm^2/electron, where the errors are 90% confidence level upper limits. The spark chamber experiment[8] obtained $\sigma(\bar{\nu}_\mu e^- \rightarrow \bar{\nu}_\mu e^-) = (5.4 \pm 1.7) \times 10^{-42}$ $E_{\bar{\nu}}$ (GeV) cm^2/electron. If this later measurement is correct, we would see $\sim$ 16 events.

II-B. Search for b Quarks and a Study of the Anomalies in the ν Inclusive Distributions

Experimental evidence exists[9] that above about 30 GeV, the naive quark model, even including charm, does not adequately describe antineutrino interactions. The rise in the ratio $\sigma_{\bar{\nu}}/\sigma_\nu$ above the value 1/3 observed at low energies[10] has been interpreted as the production of a new b quark of charge -1/3.[11] In particular, if it were to couple in a right-handed way, i.e.:

$$J_\lambda^+ = \bar{u}\gamma_\lambda (1+\gamma_5) d_c + \bar{c}\gamma_\lambda (1+\gamma_5) s_c + \bar{u}\gamma_\lambda (1-\gamma_5) b + \bar{\nu}_e \gamma_\lambda (1+\gamma_5) e + \bar{\nu}_\mu \gamma_\lambda (1+\gamma_5) \mu$$

to a valence quark, it could give rise to the observed excess events observed at large y in $\bar{\nu}$ interactions.

Cahn and Ellis[12] speculate that the mass of the b quark might be close

to 5 GeV.

Fig. 11 shows the energy distribution of our charged-current events.[13] Since the average energy is 30 GeV, we are well situated to study the apparent anomalies and probe their origin in detail. Fig. 12 shows our y distributions[13] for the complete sample and for energies greater than 30 GeV. This current data sample with its limited statistics is compatible with an anomaly (i.e. B ~ 0.5) but does not require one. One sees, however, that a measurement of B is most sensitive to high y events. Since by definition, the bulk of the energy in such events resides in the hadronic system, the improvement of the hadronic energy measurement by use of the gamma converting plates will improve our understanding of events at high y.

If $\sigma_{\bar{\nu}}/\sigma_{\nu} \simeq 0.6$ at high energy, then b-particle production could account for 30 to 40% of the $\bar{\nu}$ cross section, and so ~ 2000 events. A comparison of the anomaly for neutron and proton targets will test the hypothesis that it is due to an interaction with a valence quark. Cahn and Ellis estimate that the b quark decay channels $b \to u(\mu^- \bar{\nu})$, $b \to u(e^- \bar{\nu}_e)$, $b \to u(\bar{u}d_c)$, $b \to u(\bar{c}s_c)$, $[b \to u(\bar{U})\nu_U]$ would occur approximately in the ratios 1:1:3:1.5[:0.5] where $\bar{U}$ is a potentially observable new heavy lepton. These decays will in general have large Q values and so be reasonably conspicuous. The γ-converting plates are necessary for detecting the π^o component of the decays as well as electrons from semileptonic decays. They would substantially inprove our resolution in x, y, and E_ν for our charged-current events (see Figs. 13, 14, and 15).

II-C. $\Delta S = 1$ Reactions

The study of the two-body strangeness changing reactions over a wide

range of energy and momentum transfer will eventually form a cornerstone of the understanding of the weak interactions. For reactions involving hyperons from the baryon octet

$$\bar{\nu} p \rightarrow \mu^+ \Lambda^o \quad \text{(62 events)} \qquad \text{C1}$$
$$\hookrightarrow p\pi^-$$

$$\bar{\nu} p \rightarrow \mu^+ \Sigma^o \quad \text{(17 events)} \qquad \text{C2}$$
$$\hookrightarrow \Lambda^o \gamma$$

$$\bar{\nu} n \rightarrow \mu^+ \Sigma^- \quad \text{(48 events)} \qquad \text{C3}$$

the predicted rates in the Cabibbo model[14] are indicated. Of equal interest is a study of the reaction

$$\bar{\nu} n \rightarrow \mu^+ \Sigma^*(1385)^- \qquad \text{C4}$$
$$\hookrightarrow \Lambda^o \pi^-$$

and comparing its rate to that of

$$\bar{\nu} p \rightarrow \mu^+ \Delta^o(1238) \qquad \text{C5}$$
$$\hookrightarrow p\pi^- \quad .$$

Again, it would form a test of the Cabibbo model, and the fact that the Σ^* and Δ^o are in a decuplet means that no F/D ratio is involved.

The study of these reactions can, of course, only be carried out in a hydrogen-deuterium bubble chamber. In neon, strange particles can be produced or absorbed so readily in the nucleus as to make such measurements highly uncertain. The chief advantage of the plates in the study of these reactions will be to veto events with additional π^o's in the final state and so validate the selection techniques. They may also give a handle on separating Λ^o and Σ^o hyperons, although the low energy gamma from Σ^o decay in reaction C-2 will be difficult to detect.

The rate for inclusive reactions

$$\bar{\nu} p \rightarrow \mu^+ \Lambda^o X^o$$
$$\bar{\nu} p \rightarrow \mu^+ \Sigma^o X^o$$
$$\bar{\nu} n \rightarrow \mu^+ \Sigma^{*-} X^o$$
$$\bar{\nu} p \rightarrow \mu^+ \bar{K}^o B^o$$
$$\bar{\nu} n \rightarrow \mu^+ \bar{K}^o B^- \quad ,$$

where $X^o(B^o, B^-)$ is a nonstrange mesonic (baryonic) system, will presumably be something like 5% ($\sim \sin^2\theta_c$) of the total rate. This will mean producing approximately 700 such events. The plates system will be invaluable in detecting the π^o component of $X^o(B^o, B^-)$. To the extent that they allow a complete characterization of the final state, they will enable one to obtain a sample uncontamined by associated production.

II-D. Dileptons and the Search for Charmed Particle Production by Antineutrinos

Electronic experiments[15, 16] have observed dimuon production by neutrinos at about the one percent level. These experiments have found a similar rate for production by antineutrinos. Bubble chamber experiments[17] at FNAL have observed dilepton production by neutrinos at about the 0.6% level, but have found no clear signal in antineutrino interactions.[18] Based on a single candidate, Berge et al. report a 90% confidence upper limit for the relative yield of $\mu^+ e^-$ events as 0.5% for all charged current events with antineutrino energy greater than 10 GeV.

If the origin of the dileptons is semileptonic decays of charmed particles, then the reason for the apparent suppression in $\bar{\nu}$ interactions is not obvious. While neutrinos can produce charmed particles from the valence quarks, the process is proportional to $\sin^2\theta_c$ which is $\sim$ 0.05. The production of charmed mesons by antineutrinos must occur on antistrange quarks which should occur

at the few percent level in the nucleon sea.

Since the dominant decay of charmed particles is expected to be into hadrons, it is important to search for them in invariant mass distributions, making use of the excellent effective mass resolution of the hydrogen bubble chamber. The γ plates are likely to be vital in finding the π^0 decay products of these decays and so in completely specifying the hadronic final state.

With the addition of plates and the use of the improved External Muon Identifier, the hydrogen bubble chamber will become a highly competitive device for studying semileptonic decays of charmed particles. Electrons with momentum less than about 1 GeV will be trapped in the bubble chamber and clearly recognized. Asymmetric Dalitz decays are a principal source of potential background and are much more easily recognized in a hydrogen bubble chamber with its low density and long radiation length than in neon. The plates are necessary for recognizing higher momentum electrons. An electron crossing the set of plates will, on average, radiate more than 90% of its energy and so be clearly recognized. Typically, the electrons from neutrino-induced dilepton events appear to be produced[17] at an average transverse momentum of about 0.5 GeV/c with respect to the direction of the total hadronic system, and hence are likely to intercept the plates.

II-E. Quark Fragmentation

Next to observing quarks directly, one of the more interesting studies of them is to see how they radiate hadrons after being struck in leptonic collisions.

The hydrogen/deuterium bubble chamber can measure all final state charged hadrons and with γ-detecting plates, most of the π^o as well. This allows one to analyze the quark fragmentation in detail.[19] The parton fragmentation hypothesis is the statement that if a hadron (with 4-momentum h) is a fragment of a parton, then its momentum distribution will depend only on the invariant $Z = (h \cdot p)/(q \cdot p)$ where p is the initial 4-momentum of the target nucleon and q is the 4-momentum absorbed by the parton in the collision. In the laboratory, the variable Z reduces (e.g. for a pion fragment) to $E_\pi/(E_\nu - E_\mu)$, the ratio of the energy of the pion to the total energy transfer. Thus one regards the Z distribution as a measure of the probability distribution for a fragmenting quark to produce a hadron of fractional energy Z. From this it follows that in the current fragmentation region (large Z), the Z distribution should scale. Sehgal predicted the absolute distribution of $(Z/\sigma_T)\, d\sigma/dZ$ for pion production by antineutrinos from electroproduction measurements. Fig. 16 shows his prediction and our measurements.[13] The agreement is quite good for $Z \gtrsim 0.3$. With gamma-converting plates, we will be able to measure the fragmentation function $D_d^{\pi^o}$.

Finally, if these relations continue to work well with improved data, one can, as discussed by Sehgal,[20] use the Z distributions in neutral current events to measure the Weinberg angle.

II-F. $\bar{\nu}_e$ Interactions

The plates will also allow us to recognize interactions of the electron-type antineutrinos in the beam. Since the charged-current $\bar{\nu}_e$ interactions should have a $(1-y)^2$ distribution, the resulting positrons will nearly all intercept the plates and be recognized. We estimate that there will be approximately

120 such events in the exposure. Their study will allow a test of μ-e universality at high energy and momentum transfer.

II-G. Quark Distribution Functions

By using deuterium as a target, and γ plates in order to improve the hadronic energy resolution, it is possible in one experiment to measure the absolute value (not just the shape) of the ratio of the down-to-up quark distributions as a function of x. For x values greater than $\sim$ 0.2 (when the sea contributions are small), one has

$$R = \frac{d(x)}{u(x)} = \left(\frac{d\sigma}{dx}\right)_{\bar{\nu}n} / \left(\frac{d\sigma}{dx}\right)_{\bar{\nu}p} \quad .$$

Many theorists regard the large x behavior of this ratio to be of high importance, but are not able to make unique predictions. For example, R. Feynman[23] predicts $R \to (1 - x)^4 \to 0.0$ as $x \to 1.0$, while G. Farrar[24] predicts that $R \to 0.20$; a precise measurement in the range $x > 0.60$ would be of great value in resolving this question. In Feynman's model, there would be $\sim$ 50 $\bar{\nu}n$ events and $\sim$ 600 $\bar{\nu}p$ events with $x \geq 0.6$ in 500K deuterium pictures.

III. Gamma Converting Plates

A. Suggested Plate Arrangement

We propose to install a set of four closely spaced plates in the downstream region of the bubble chamber as shown in Fig. 1. In particular, we suggest using four tantalum plates, each 0.5 conversion lengths thick and separated by 9-inch in the median plane. Thus for a fiducial volume upstream of the plates, most gammas would go through the complete set of plates. This configuration has a 90% probability of converting γ's that transverse the set at normal incidence, and higher probabilities at other angles.

Of course, some gammas will come off at large angles from interactions occurring far upstream in the bubble chamber and will miss the plates. However, these gammas will generally have low energy and so their loss will not be crucial in most applications. Fig. 17 shows our observed laboratory momentum angle distribution from E(31) for gammas that convert in the hydrogen. The three highest energy gammas were observed to have ~ 15, 12, and 8 GeV and go within ~ 5 degrees of the $\bar{\nu}$ beam direction, while at large angles, i.e. greater than 30 degrees, the typical momenta are less than 500 MeV/c. Since the statistics on Fig. 17 are sparse, we shown in Fig. 18 the laboratory momentum-angle distribution for observed π^- in E-31. One can use it to simulate the π^o distribution. Since on the average, the two gammas from the π^o decay share equally the π^o momentum, it confirms the expectation that a downstream system of plates will convert the bulk of the produced gammas. Table II shows the probability of converting N gammas out of the total N_γ present in the final state. To summarize it by a single number, we find that we will observe 65% of all final state gammas for a fiducial volume upstream of the plates, and a much larger percent of the neutral energy carried by gammas. We previously suggested the addition of such plates in our proposal for E(390). A similar downstream plate arrangement was proposed[21] for the BEBC chamber at the SPS.

III. B The Use of Downstream Gamma Converting Plates to Recognize Final State Baryons and Measure Their Momenta

If an antineutrino interaction contains a final state proton, one would like to pick it out from final state π^+ mesons. If it contains a final state neutron one wishes, if possible, to detect it and to measure its momentum. This measurement of final state nucleons is important for completely characterizing the hadronic

system for all reactions, and in particular for determining the incident neutrino energy in neutral current interactions.

In general, one cannot recognize a final state positive particle as a proton or a π^+ in neutrino or antineutrino interactions. Since 80% of the protons have momenta greater than 1 GeV/c, they and the pions are both generally minimum ionizing.

A set of downstream plates is useful if the track in question interacts upstream of them. In about half the proton interactions, a final state neutron will carry off the bulk of the momentum ($\sim$ 60%).[22] The neutron will, of course, not cause an electromagnetic shower in the plates. Hence, a signature of a proton would be a positive track that interacts with a substantial loss of visible momentum and no associated high energy gammas converted in the plates. Concentrating the plates downstream increases the probability of a proton interacting upstream of them. The absorption length of 3.4 m for protons in deuterium means that the typical proton will interact upstream of the first plate about 30% of the time.

In addition, for neutrons which interact upstream of the plates, the γ conversion will substantially enhance one's ability to measure their momenta. In particular, this is true if the neutron collision produces a neutron and one or more π^o's. Such reactions would otherwise be under-constrained.

III. C Another Plate Arrangement

An alternate proposal has called for distributing the plates uniformly in the chamber. While this has the advantage of having the plates subtend a larger solid angle it also has several severe drawbacks. The problems chiefly revolve around the possibility that one or more

of the hadrons in the final state will interact in one of the upstream plates. For example, in a scheme which has the plates spaced at 1-foot intervals, the average primary vertex would be only 6 inches from the first plate. If a hadron interacted there, it would be difficult to tell if downstream K^o, Λ^o, and converted γ were to be associated with the primary vertex or the interaction in the plate. Further, if the interaction in the plate cascaded in the nuclear material to produce a large multiplicity of charged particles, they would enormously complicate the analysis of particles from the primary vertex. The third problem involves the danger that small angle hadronic scattering in a plate will be undetected in measurement and give an incorrect momentum measurement. Finally, the conversion of a γ near the primary interaction point will result in further confusion. It will be difficult to tell if other downstream γ's originate from it or from the primary vertex, which could confuse even a rudimentary measurement of the number of γ's in the final state. We estimate that the distributed plates would convert ~80% of all final state gammas, as compared to 65% in our case.

III. D Plate Material and Mounting

The primary consideration in choosing material for gamma converting plates is to increase the gamma conversion probability (which goes as Z^2) while minimizing the probability of hadron interaction (which goes as $A^{2/3}$). For a downstream plate configuration, the problem of needing to measure hadrons through the plates is virtually eliminated. However, two fundamental problems remain. First, if a hadron track interacts in a plate, it will produce a number of charged and neutral hadrons. The hadron tracks generate confusion and the π^o's will give rise to converted gammas that must be separated from locally converting gammas that originated from the primary vertex. The second

problem is that of Λ^o and K_s^o detection. One wishes to have these particles decay and be clearly measured, rather than interact in the plates. One reduces both of these problems by making use of high Z plates localized downstream.

With regard to the accuracy of gamma measurement, one wishes to maximize the conversion probability of the gamma and minimize the energy loss of the created electron positron pair. To first order this cannot be done since the conversion length and radiation length are in the fixed proportion of 9/7. A second order effect again favors high Z materials since the inverse conversion length goes as Z^2 while dE/dx for electrons goes as Z. This difference is likely to be important for low energy gammas such as will occur in the reaction $\bar{\nu} p \rightarrow \Sigma^o \mu^+$, $\Sigma^o \rightarrow \Lambda^o \gamma$.

The best plate material appears to be tantalum. It has high Z(73), is readily available, and has good mechanical properties.

The experimenters submitting this proposal are fabricating a similar set of tantalum plates for their ν experiment in the 12-foot bubble chamber at Argonne National Laboratory. Fig. 19 shows that plate arrangement. Our experience with the plates in the 12-foot chamber should prove invaluable. Finally, the tantalum plates from the 12-foot bubble chamber experiment will be available for use in this experiment.

References

1. J. J. Sakurai, Erice Conference 1976, UCLA/76/TEP/21.

2. A. Benvenuti et al., Phys. Rev. Lett. 37, 1039 (1976); B. C. Barish et al., at 1976 Neutrino Conference, Aachen NU-76-51 and CALT 68-563.

3. P. Schreiner, Aachen Neutrino Conference, June 1976, ANL-HEP-CP-76-43.

4. Hung and Sakurai, Phys. Letters 63B, 295 (1976).

5. L. Wolfenstein and D. Wyler, Carnegie-Mellon Preprint COO-3066-77.

6. B. W. Lee Summary talk, 1976 Neutrino Conference Aachen.

7. J. Blietschan et al., Nucl. Phys. (to be published).

8. F. Bobisut et al. in Neutrino Conference, Aachen 1976 (to be published).

9. A. Benvenuti et al., Phys. Rev. Letters 37, 1095 (1976).

10. A. Benvenuti et al., Phys. Rev. Letters 37, 189 (1976).

11. R. M. Barnett, Phys. Rev. Letters 36, 1163 (1976) and Phys. Rev. D14, 701 (1976); V. Barger, J. Weiler, and R. J. N. Phillips, Phys. Rev. D14, 1276 (1976), R. M. Barnett, H. Georgi, and H. D. Politzer, Phys. Rev. Letters 37, 1313 (1976).

12. R. N. Cahn and S. D. Ellis, University of Michigan preprint UMHE 76-45.

13. M. Derrick, Aachen Neutrino Conference, June 1976, ANL-HEP-CP-76-42.

14. Cabibbo and Chilton, Phys. Rev. 137B, 1628 (1965) and Eichten et al, Phys. Letters 40B, 593 (1972).

15. B. Aubert et al., Proc. XVII Conference on High Energy Physics (London) 1974. A Benvenuti et al., Phys. Rev. Letters 34, 419 and 597 (1975).

16. B. Barish et al., Phys. Rev. Letters 36, 939 (1976).

17. J. VonKrogh et al., Phys. Rev. Letters 36, 710 (1976), J. VonKrogh, Proc. Madison Conference (April 1976), C. Baltay, 1976 DPF Meeting at Brookhaven.

18. J. P. Berge et al., Fermilab preprint 76/81-EXP, submitted to Phys. Rev.

19. L. M. Sehgal, Nucl. Phys. B90, 471 (1975).

20 J. Cleymans and L. M. Sehgal, Nucl. Phys. B74, 285 (1974).

21. L. Behr et al., LPNHE-Ecole Polytechnique-Paris, CERN/SPSC/74-119/P 33, November 21, 1974.

22. D. Dekkers et al., Phys. Rev. 137B, 962 (1965).

23. R. Feynman, Photon-Hadron Interactions, W. A. Benjamin (1972).

24. G. R. Farrar, private communication.

Table I: Total Events ($\bar{\nu}$d)
(for 500,000 pictures based on measured event rates from E31 and 1.5×10^{13} ppp)

A. Charged Currents
Inclusive Reactions

1. Multiplicity distribution for $\bar{\nu}_\mu$p

Number of Charged Tracks	Events
1	1600
3	4700
5	3400
7	1000
9, 11, 13	300

2. Total $\bar{\nu}_\mu$p Charged Current (C. C.) Events	11,000
3. Total $\bar{\nu}_\mu$n C. C. Events	5,500
4. Total $\bar{\nu}_\mu$ C. C. Events	16,500
5. Total $\bar{\nu}_\mu$ C. C. Events with $E_{\bar{\nu}} > 30$ GeV	5,500
6. Total $\bar{\nu}_e$ C. C. Events	~ 120

B. Neutral Currents

Inclusive Reactions assuming R = 0.45	Events
1. $\bar{\nu}$p + $\bar{\nu}$n	7,425
2. $\bar{\nu}$p + $\bar{\nu}$n (with measured final state nucleon)	~2,000

Table II. Fid. Vol. Upstream of the Plates
(probability of a single γ converting is 0.65)

N_γ	$N = N_\gamma$	$N = N_\gamma - 1$	$N = N_\gamma - 2$	$N = N_\gamma - 3,\ N_\gamma - 4,\ \ldots\ 0$
2	.422	.456	.122	
4	.178	.384	.310	.128
6	.075	.244	.328	.353
8	.032	.137	.259	.572
10	.013	.072	.176	.739

Figure Captions

Fig. 1 Side view of 15' chamber showing downstream plate arrangement. Plates are each 0.5 conversion lengths of Tantalum.

Fig. 2 Ratio of $\bar{\nu}p$ neutral current inclusive cross section to charged current inclusive cross section ($R^{\bar{\nu}p}$) vs. ratio of νp neutral current inclusive cross section to charged current inclusive cross section ($R^{\nu p}$). The experimentally determined relationship is shown as the solid line along with the estimated errors. The prediction of the Weinberg-Salam model is also indicated.

Fig. 3 The expected resolution in x for neutral current events with the downstream plate arrangement. The momentum of the final state nucleon was assumed to have been measured. The energy resolution for the converted gammas was taken to be ± 30%. Multiple scattering for the charged tracks was not included since for our configuration it would be nearly the same whether or not the plates are in place.

Fig. 4 The expected resolution in the hadronic energy for neutral current events with the downstream plate arrangement.

Fig. 5 The expected resolution in the hadronic momentum for neutral current events with the downstream plate arrangement.

Fig. 6 The expected resolution in the angle of the total hadronic momentum vertex with the incident antineutrino direction for neutral current events with the downstream plate arrangement.

Fig. 7 The expected resolution in the incident antineutrino energy for neutral current events with the downstream plate arrangement. The momentum of final state nucleon is assumed to be measured.

Fig. 8 The expected resolution in y for neutral current events with the downstream plate arrangement. The momentum of the final state nucleon is assumed to be measured.

Fig. 9 The ratio of the $\bar{\nu}$n inclusive cross section to the $\bar{\nu}$p inclusive cross section as a function of x for various forms of the neutral current interaction.

Fig. 10 Neutrino-electron elastic cross sections as a function of the sine squared of the Weinberg angle.

Fig. 11 The energy distribution of the observed $\bar{\nu}$p charged current events in E31.

Fig. 12 The y distributions of the observed $\bar{\nu}$p charged current events in E31.

Fig. 13 The expected resolution in x for charged current events with and

without downstream plates.

Fig. 14 The expected resolution in y for charged current events with and without downstream plates.

Fig. 15 The expected resolution in the incident antineutrino energy with and without downstream plates for charged current events.

Fig. 16 The Z distribution for inclusive pion production by antineutrinos. (Data from E31).

Fig. 17 The laboratory momentum versus scattering angle for observed gammas in E31.

Fig. 18 The laboratory momentum versus scattering angle for observed negative pions in E31.

Fig. 19 The plate arrangement in the 12 foot ANL bubble chamber.

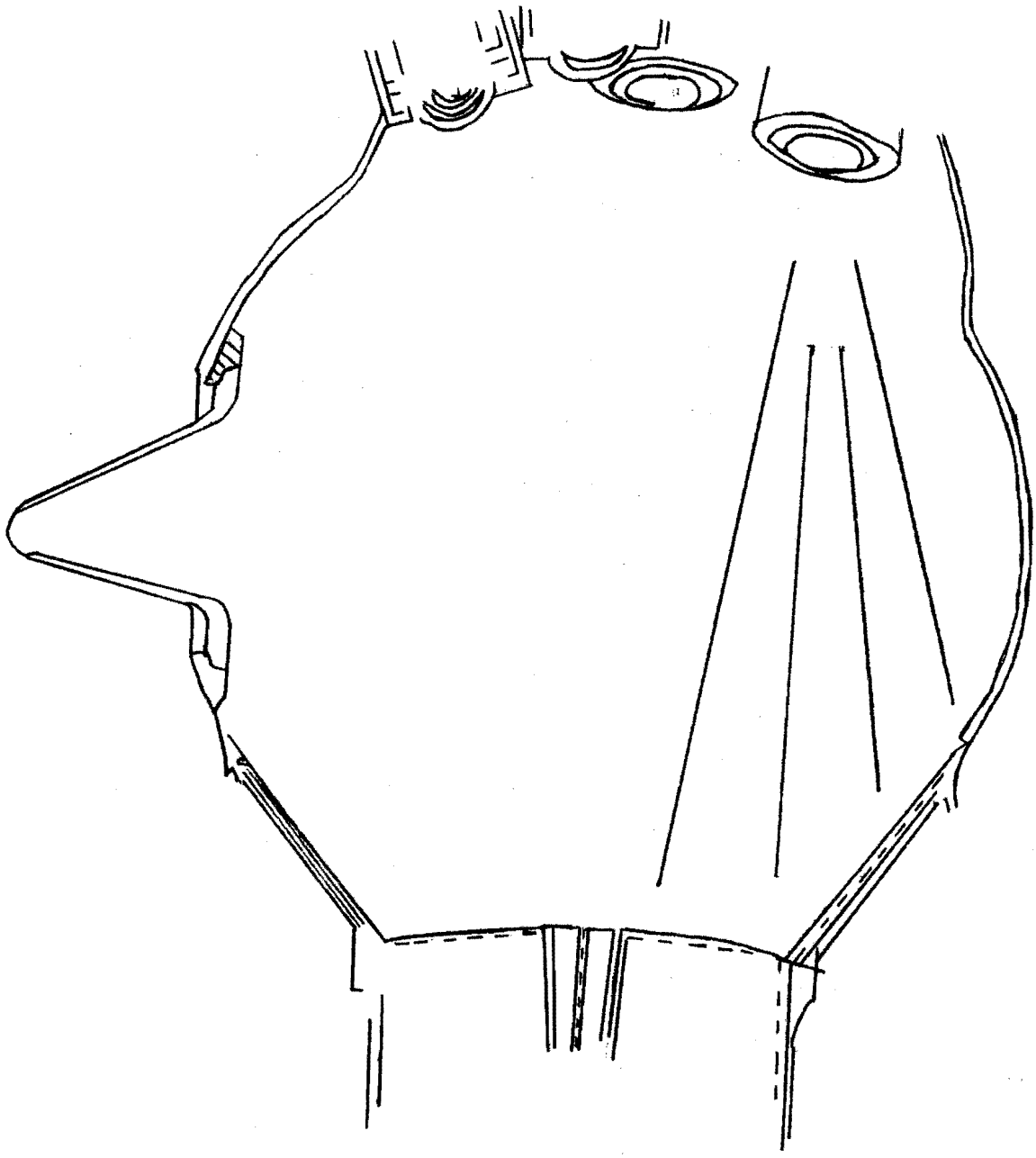

Figure 1

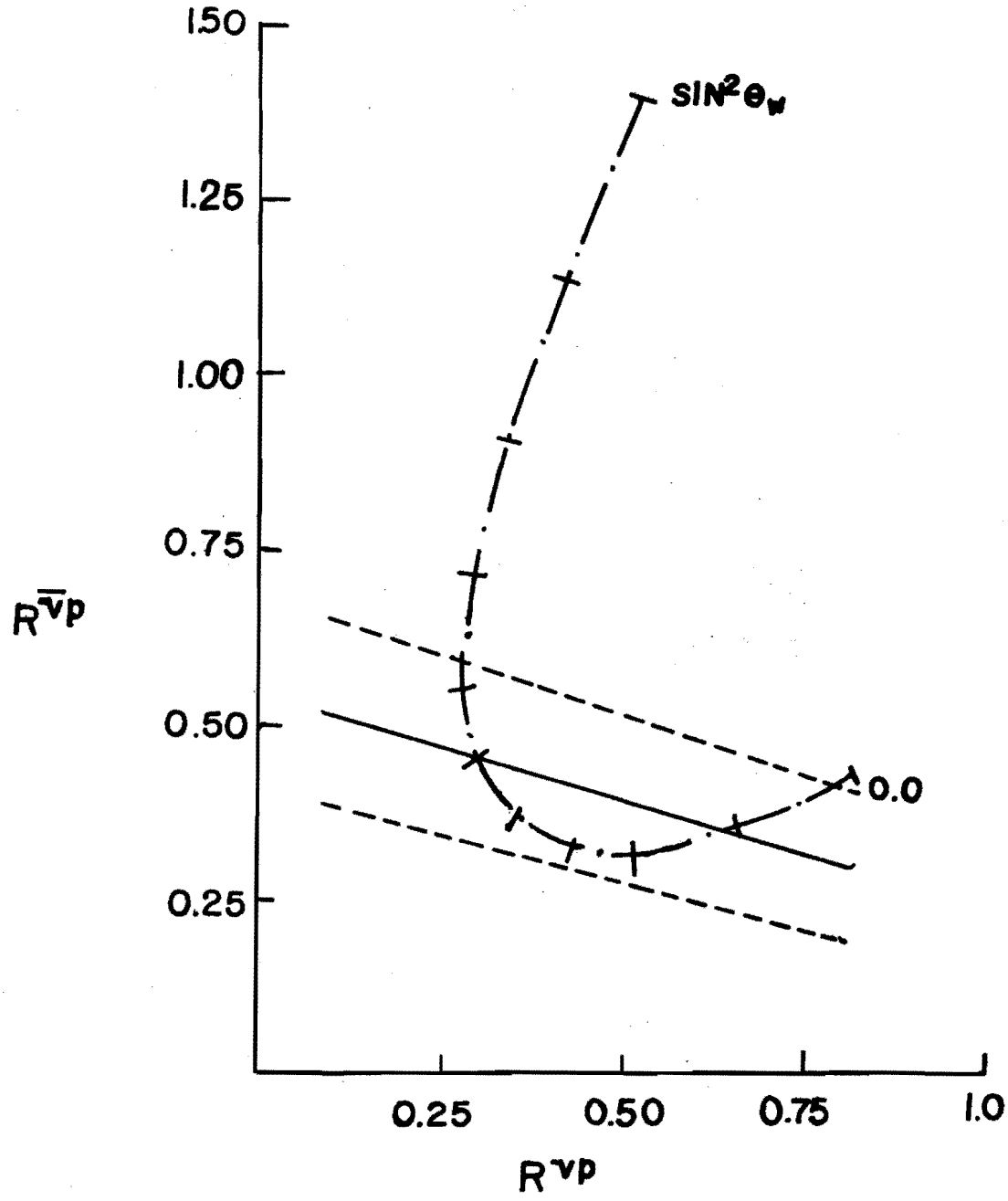
1.50
1.25
1.00
0.75
0.50
0.25
$R^{\bar{\nu}p}$
$\sin^2\theta_W$
0.0
0.25
0.50
0.75
1.0
$R^{\nu p}$

Figure 2

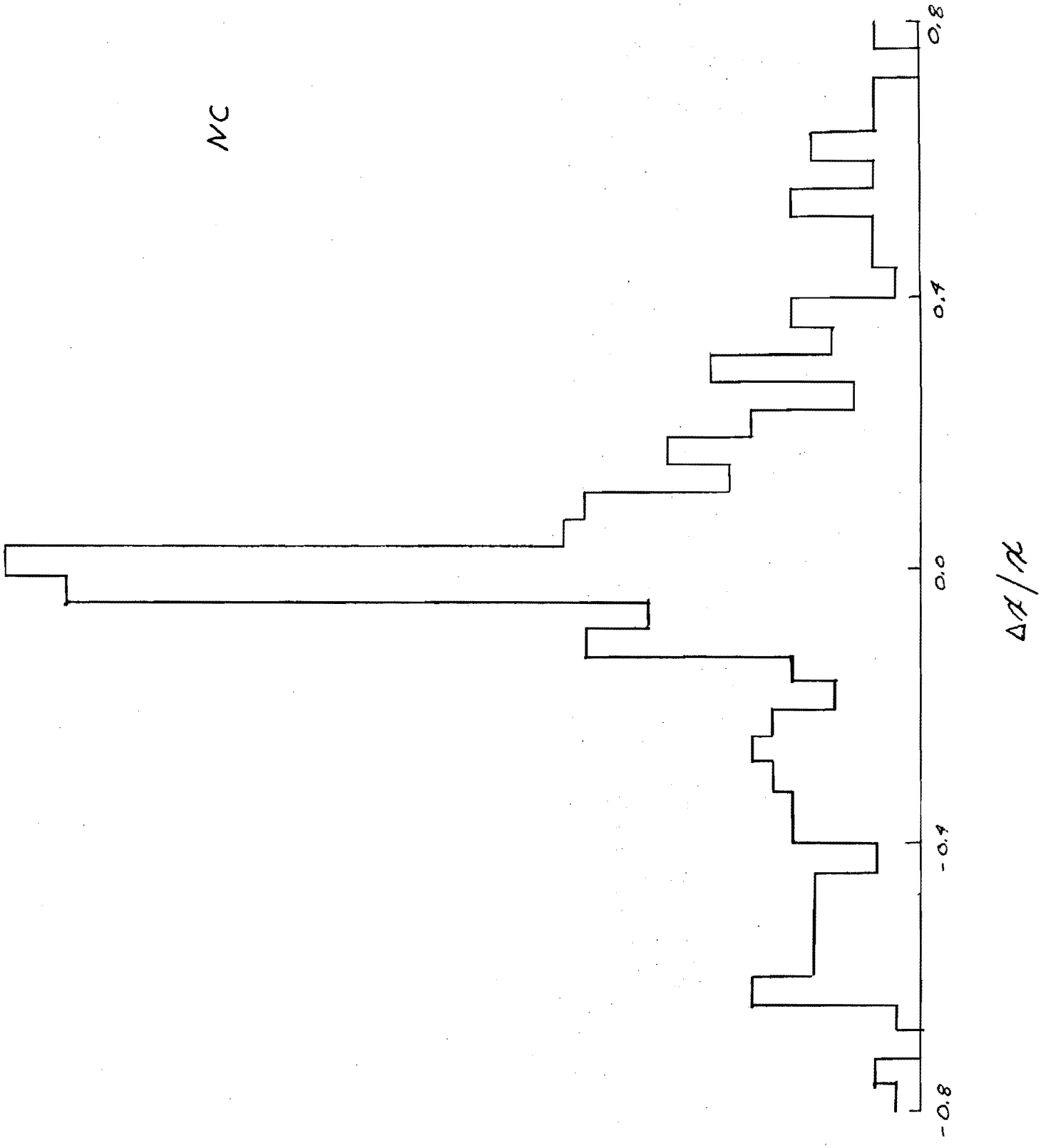

Figure 3

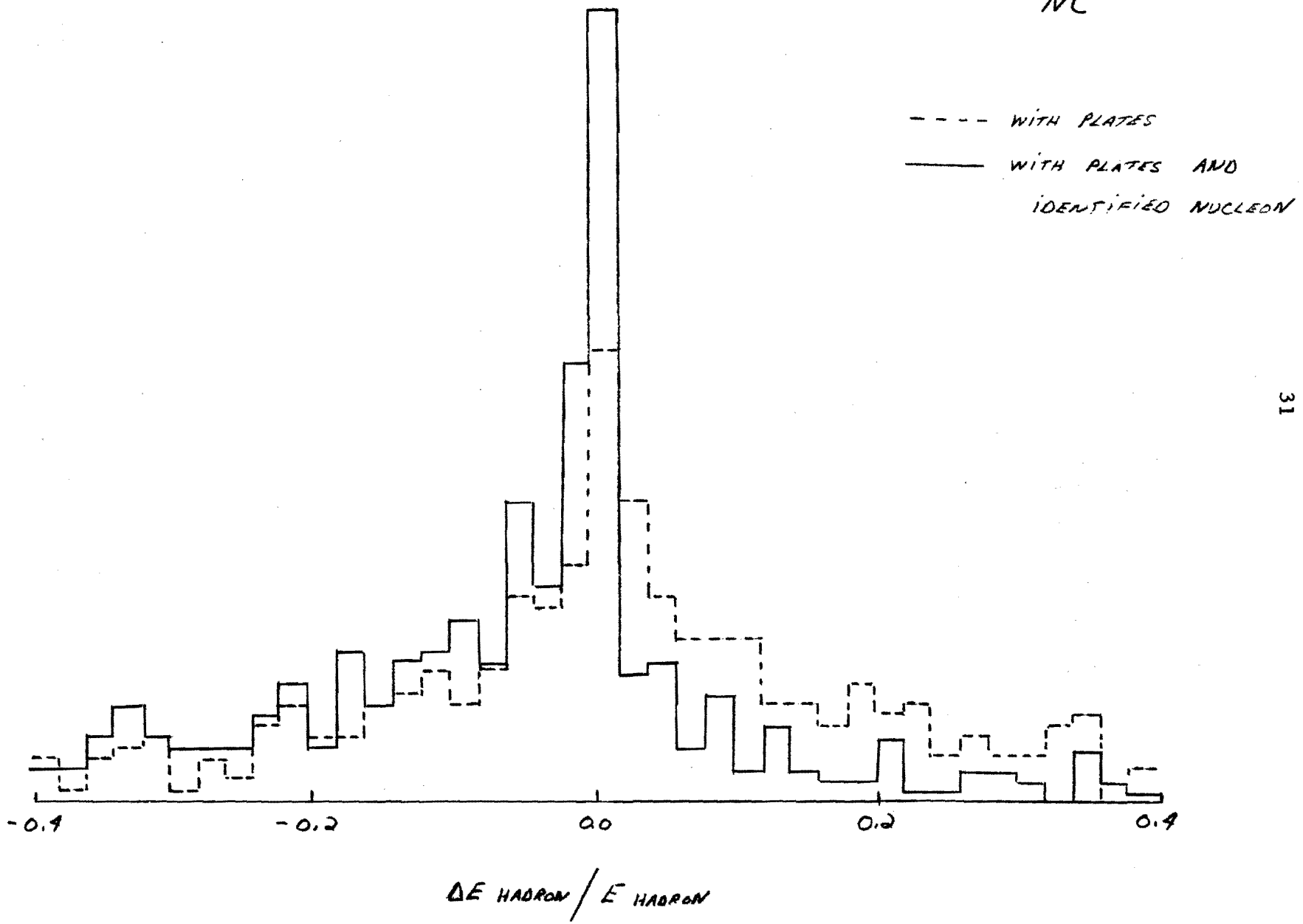
NC
WITH PLATES
WITH PLATES AND
IDENTIFIED NUCLEON
-0.4
-0.2
0.0
0.2
0.4
ΔE HADRON / E HADRON

Figure 4

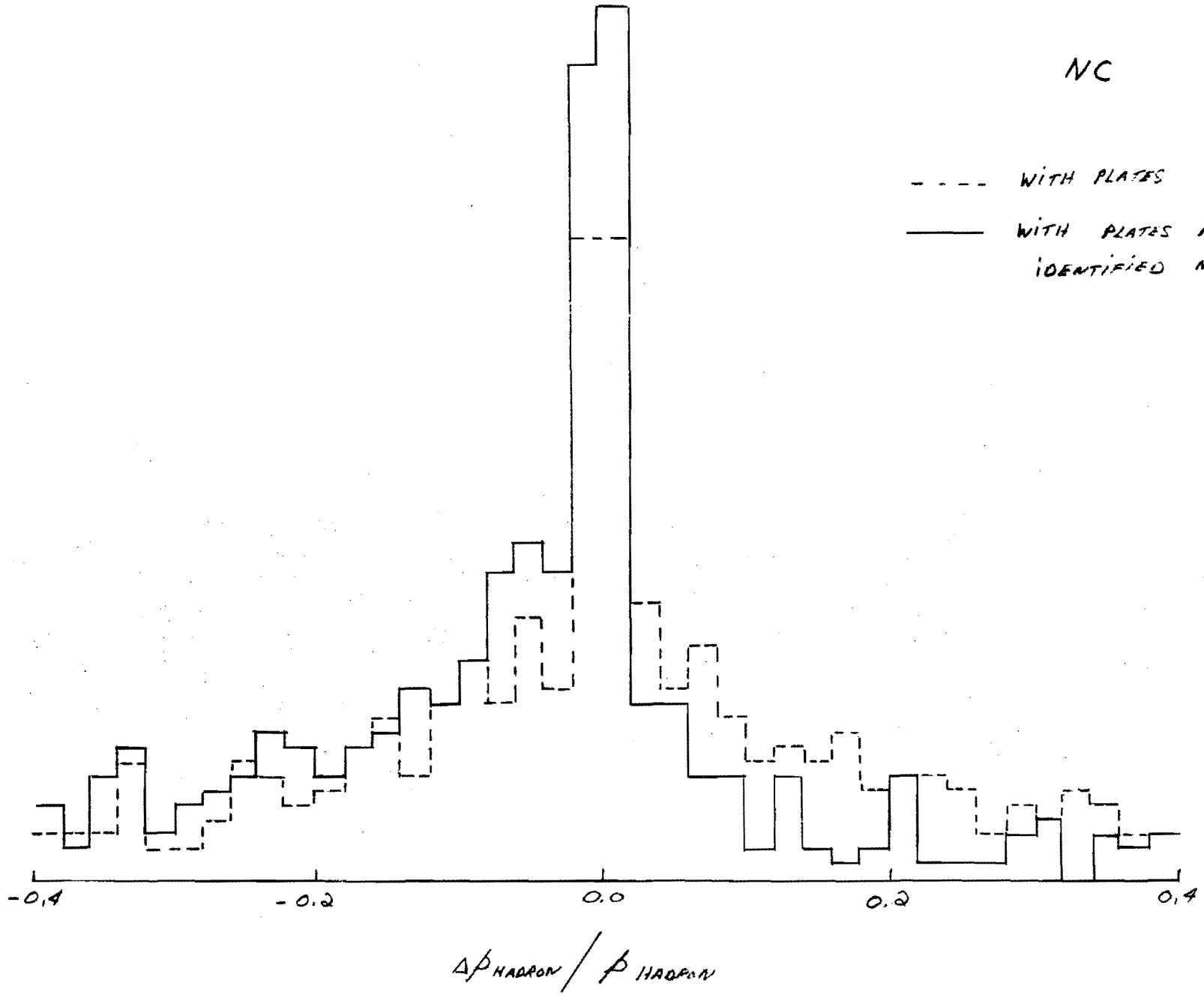
NC
WITH PLATES
WITH PLATES AND IDENTIFIED NUCLEON
-0.4
-0.2
0.0
0.2
0.4
Δp HADRON / p HADRON

Figure 5

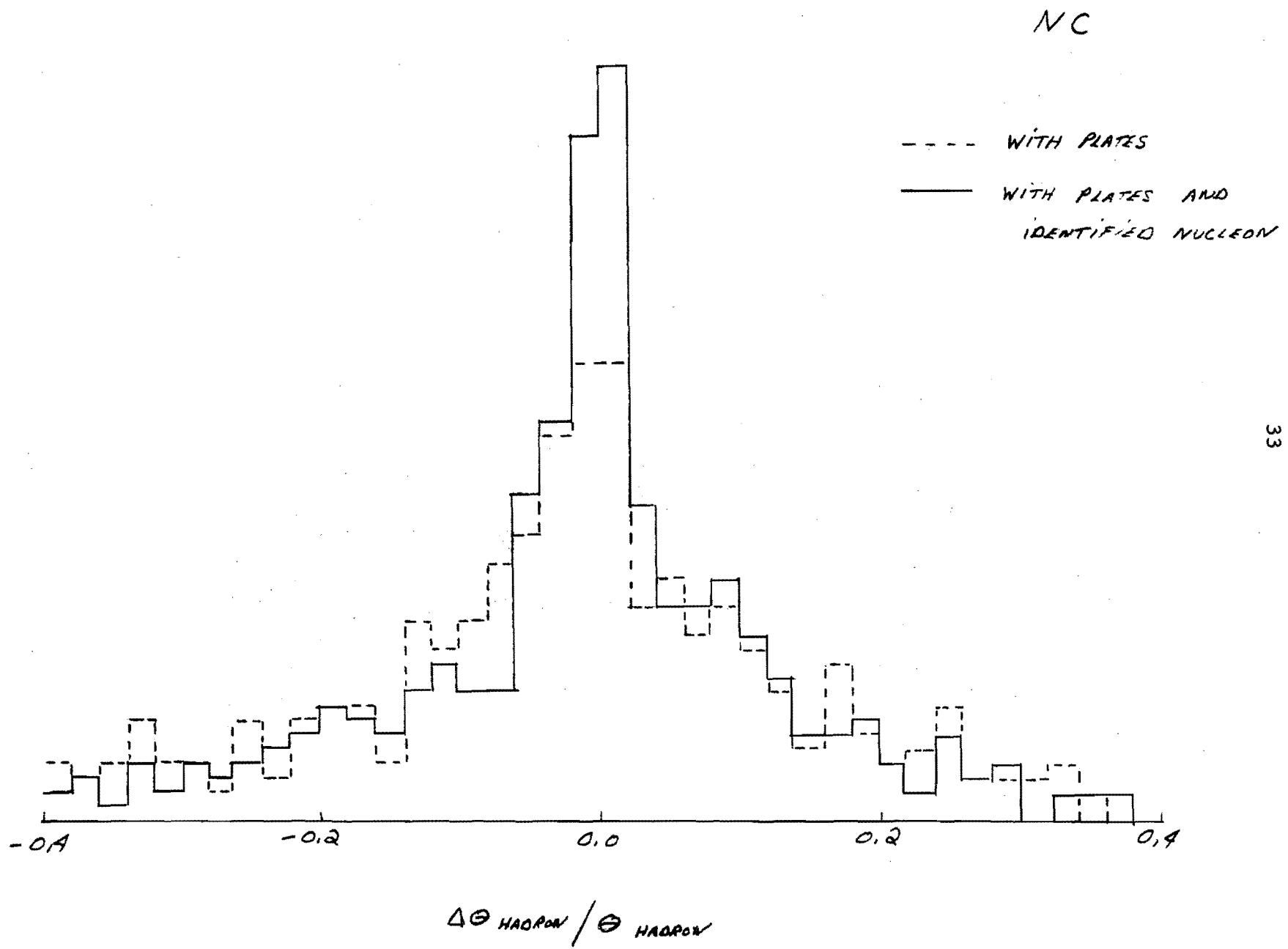
NC
WITH PLATES
WITH PLATES AND IDENTIFIED NUCLEON
-0.4
-0.2
0.0
0.2
0.4
Δθ HADRON / θ HADRON

Figure 6

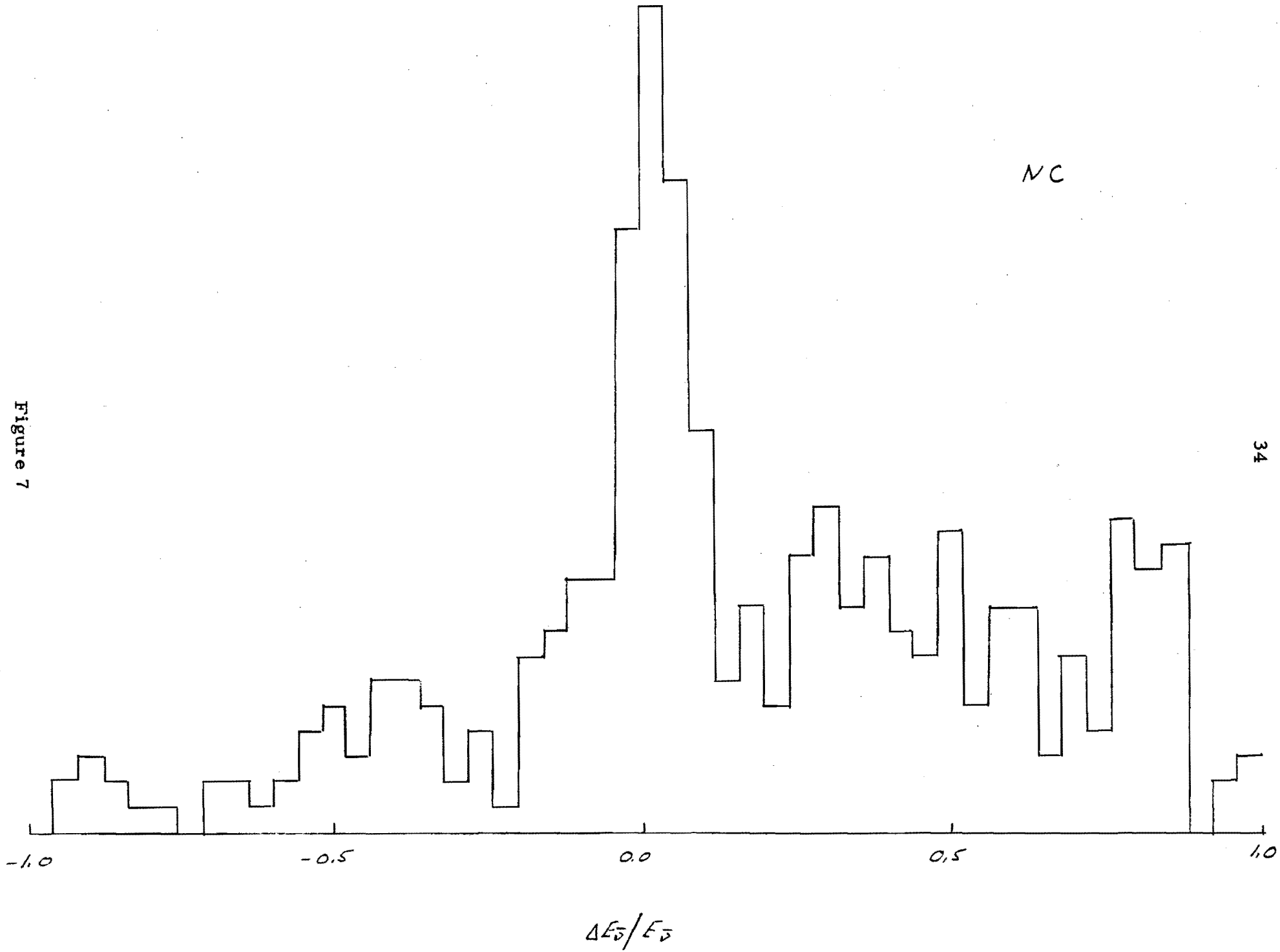

Figure 7

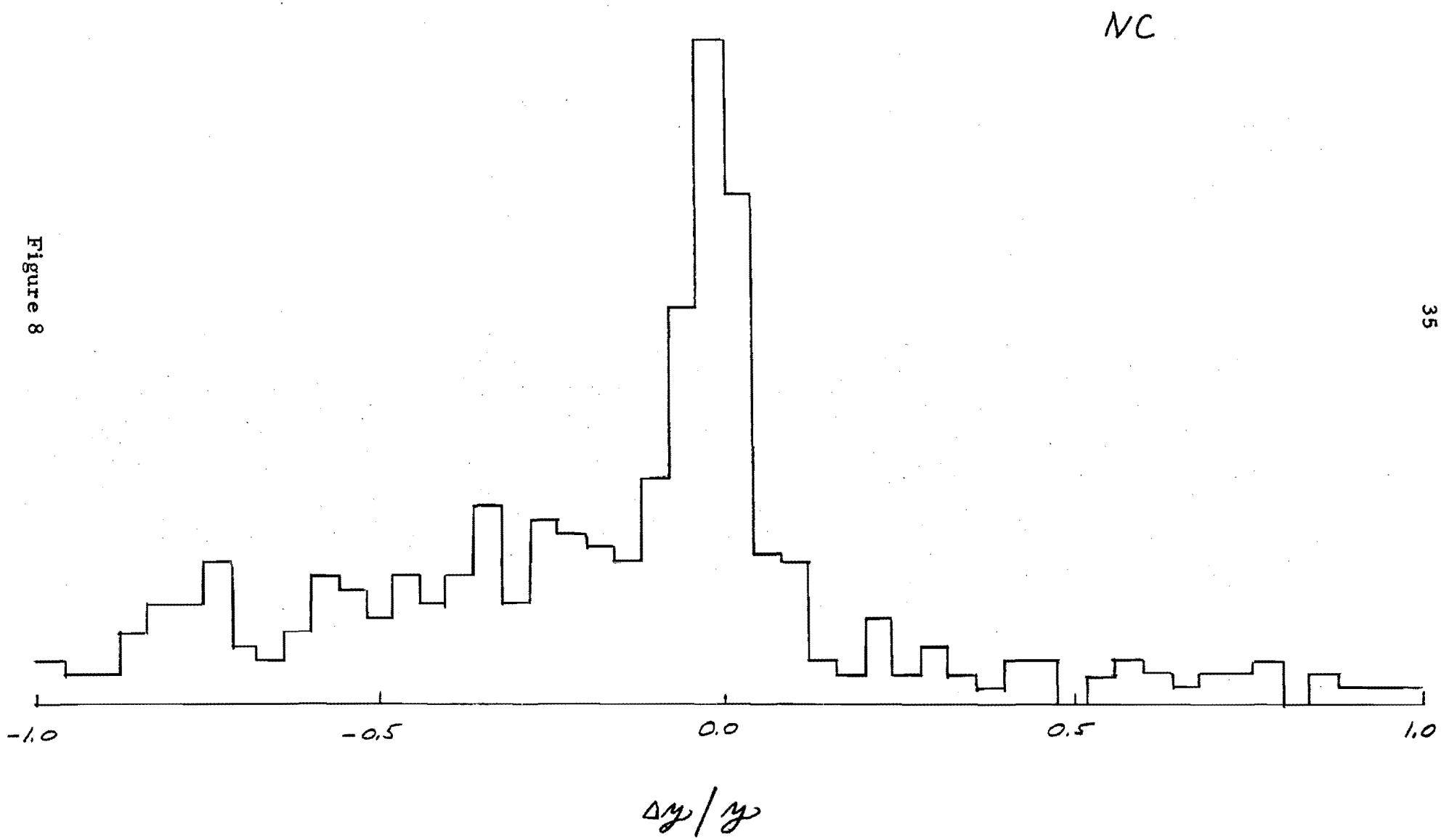

Figure 8

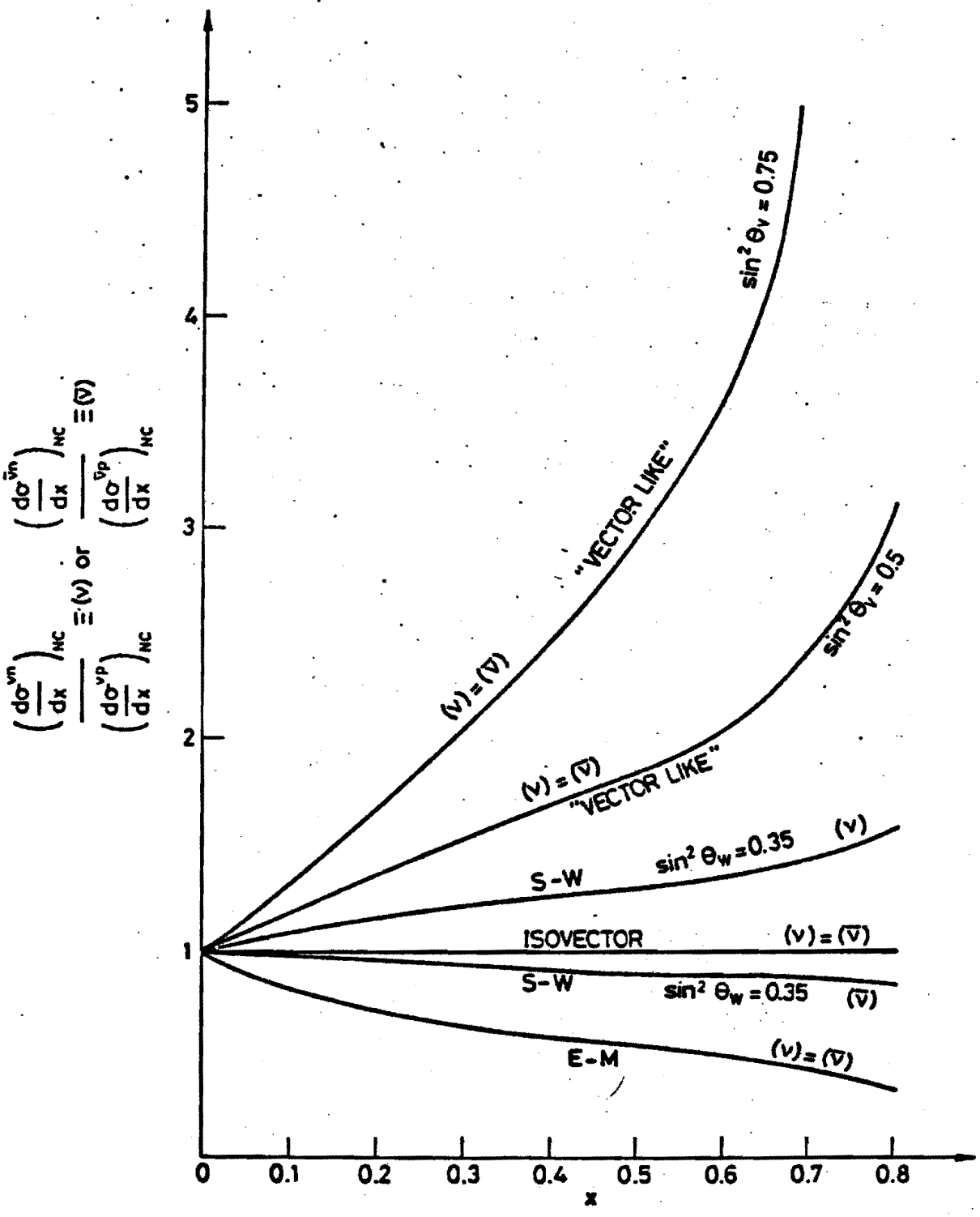

Figure 9 Cross section ratios in the inclusive reactions

Variation with $\sin^2 \theta_W$ of cross-sections
for the different ν-e processes.

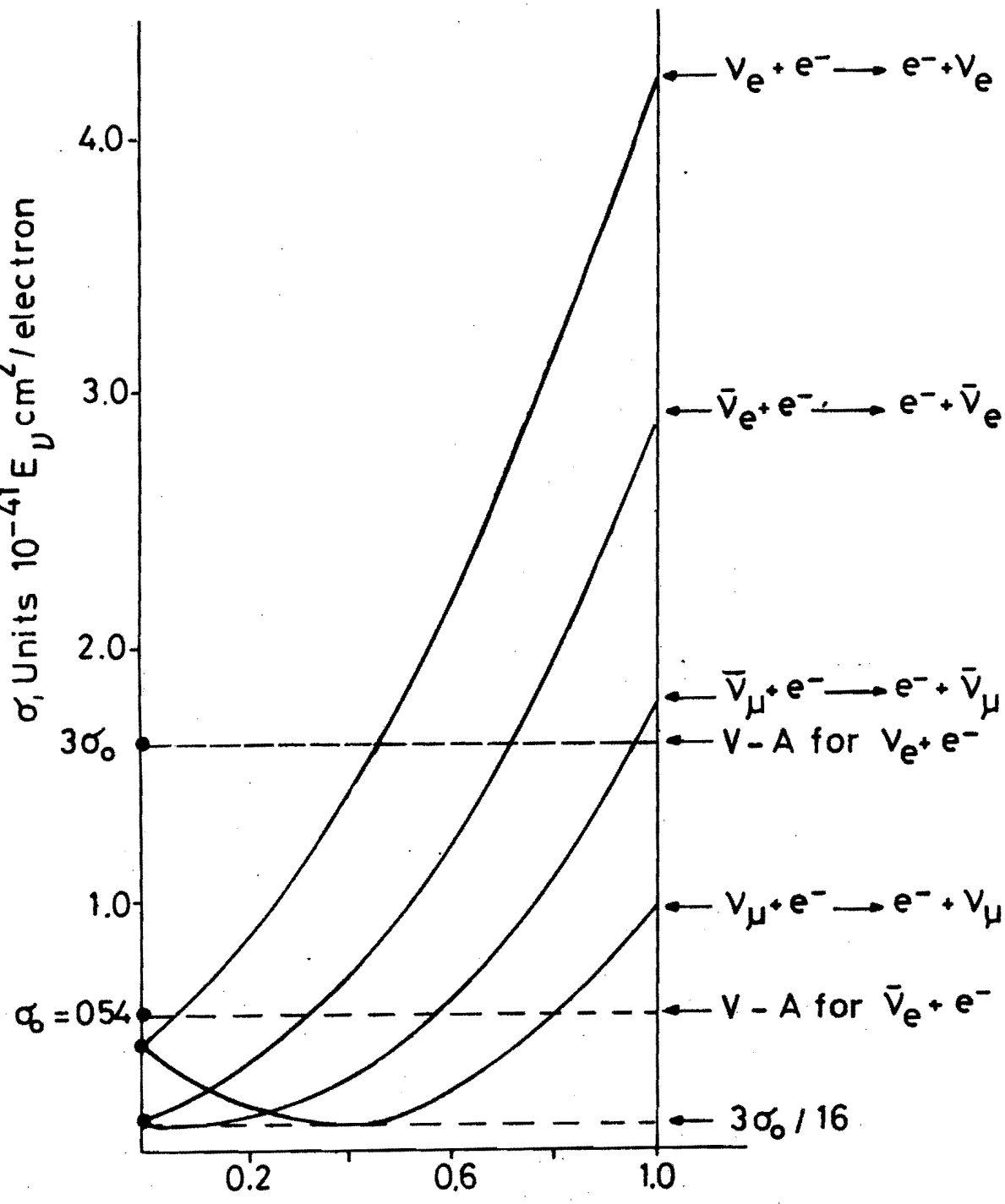

Figure 10

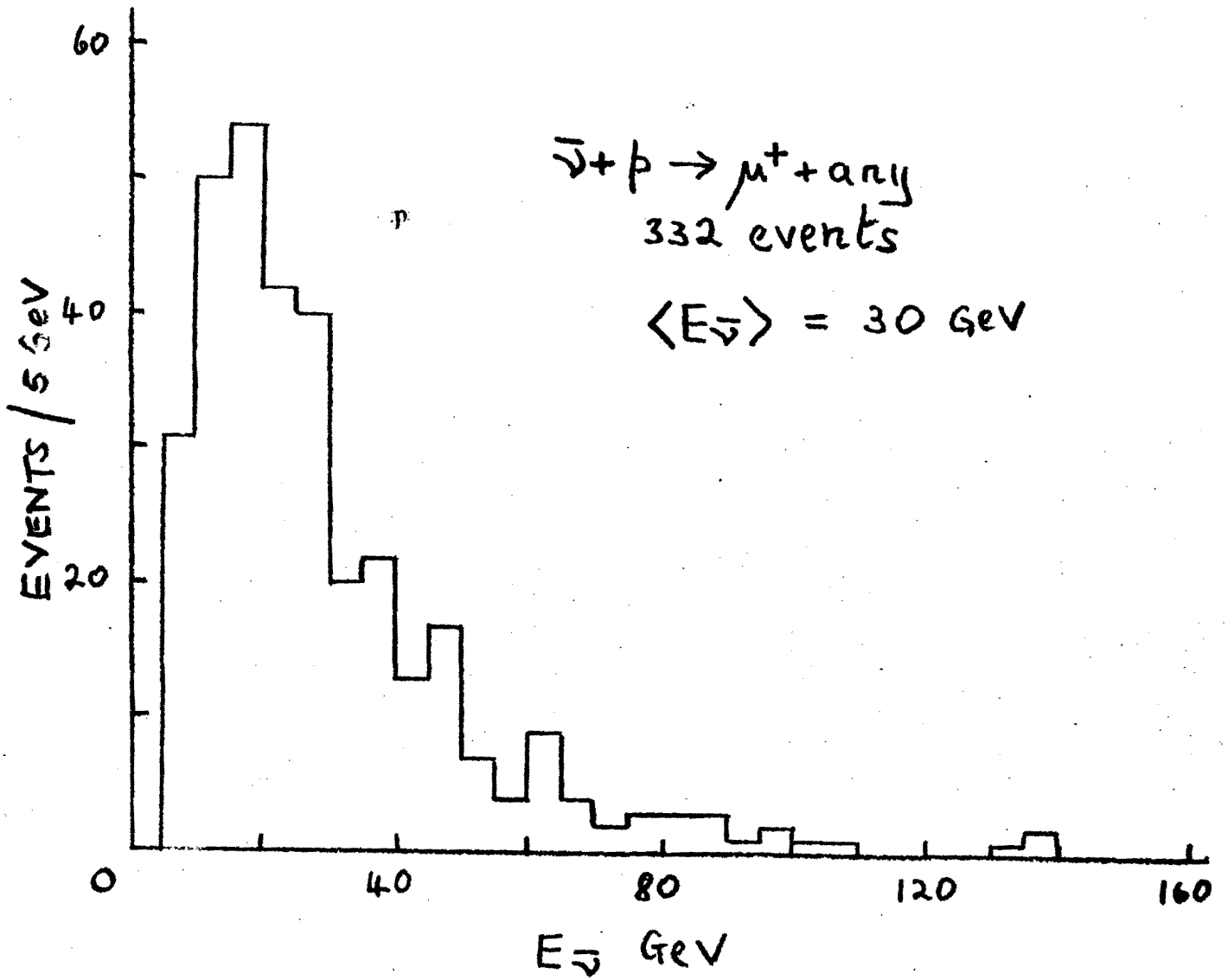
60
40
20
0
EVENTS / 5 GeV
40
80
120
160
$E_{\bar{\nu}}$ GeV
$\bar{\nu} + p \rightarrow \mu^+ + any$
332 events
$\langle E_{\bar{\nu}} \rangle$ = 30 GeV

Figure 11

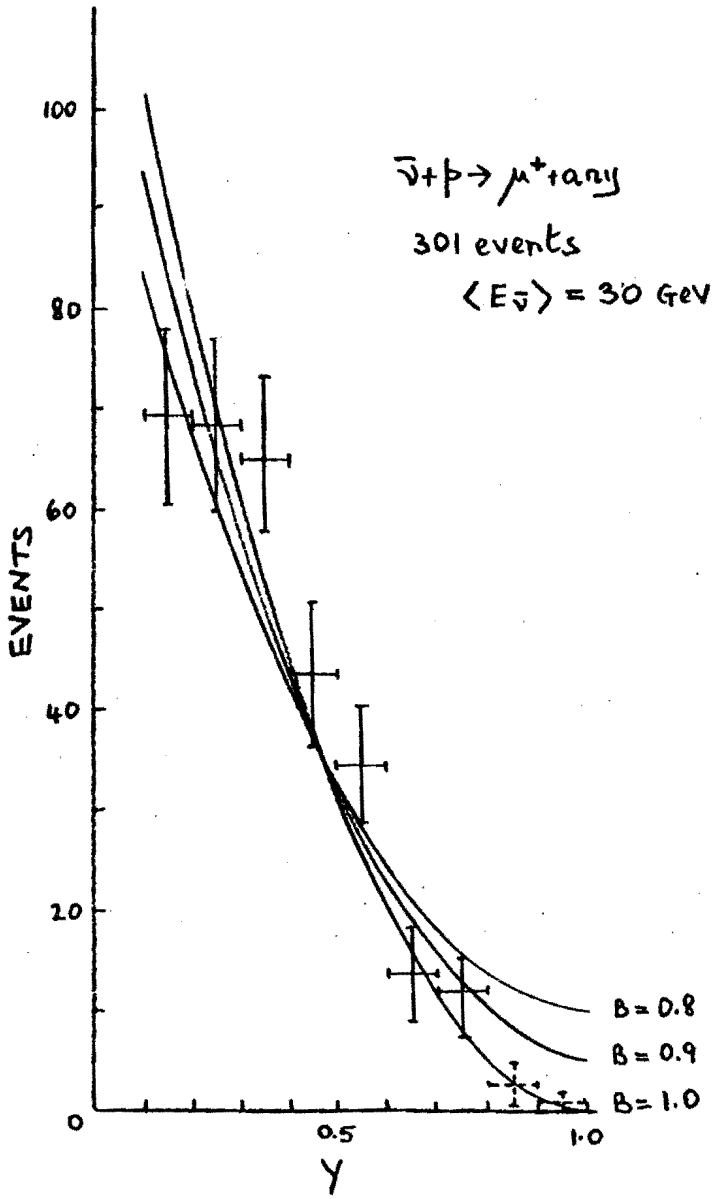
$\bar{\nu}+p \to \mu^+ + any$
301 events
$\langle E_{\bar{\nu}} \rangle = 30$ GeV
EVENTS
Y
B = 0.8
B = 0.9
B = 1.0
0
20
40
60
80
100
0.5
1.0

Figure 12

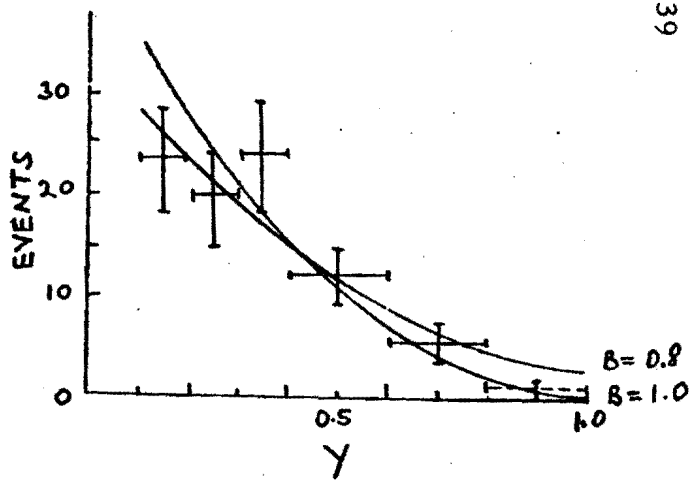
$\bar{\nu}+p \to \mu^+ + any$
104 events, $E_{\bar{\nu}} > 30$ GeV
$\langle E_{\bar{\nu}} \rangle = 52$ GeV
EVENTS
Y
B = 0.8
B = 1.0
0
10
20
30
0.5
1.0

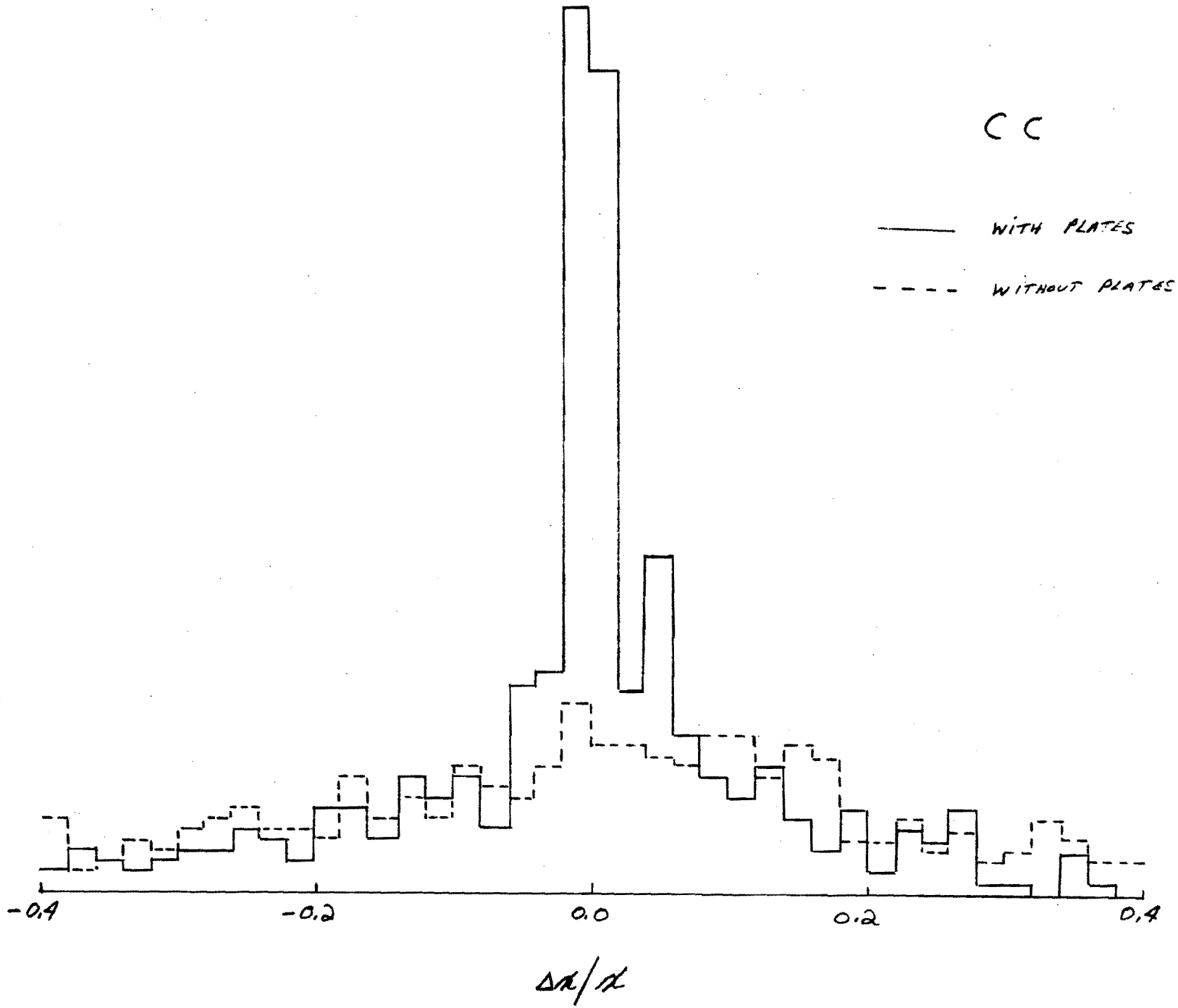

Figure 13

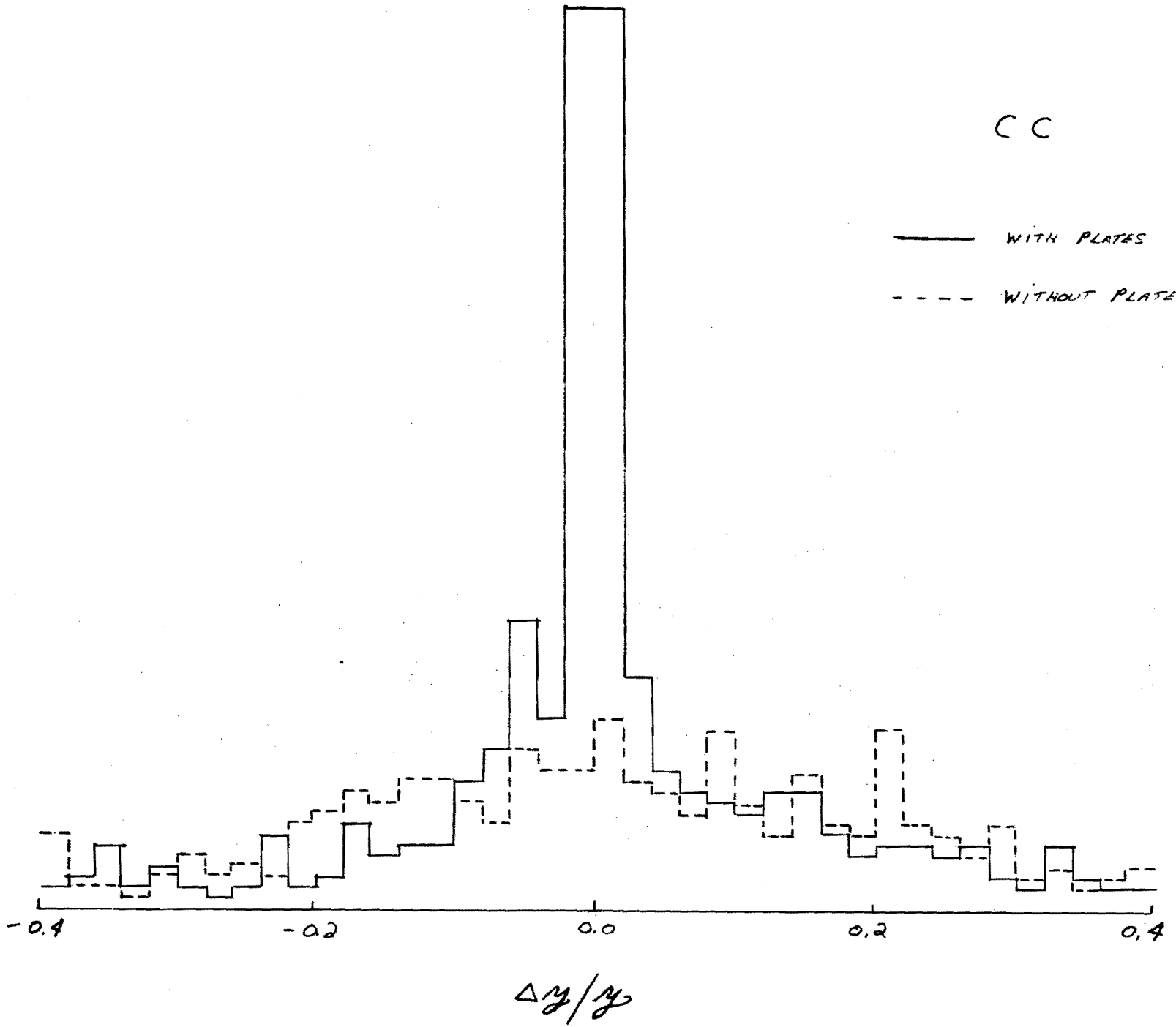

Figure 14

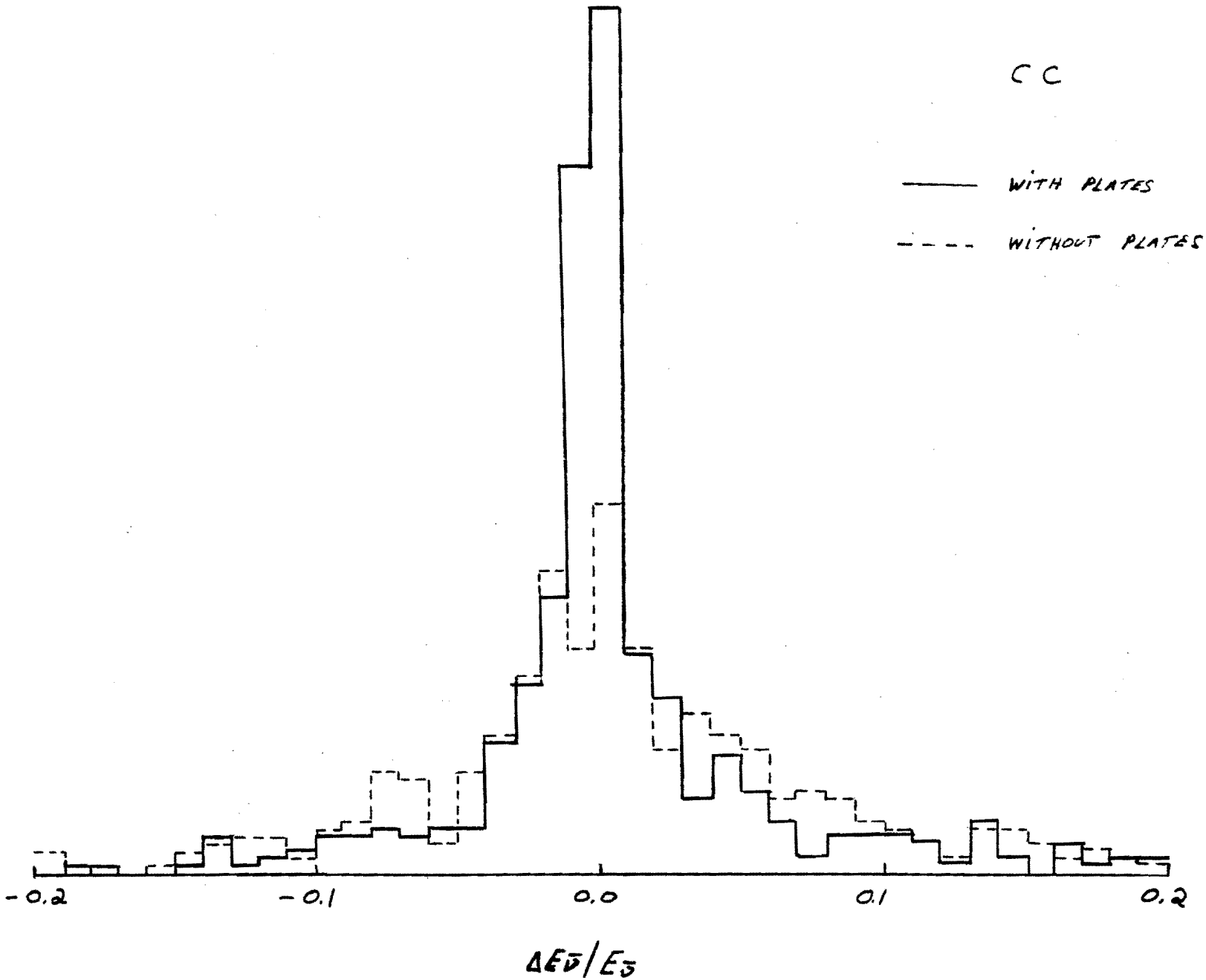

Figure 15

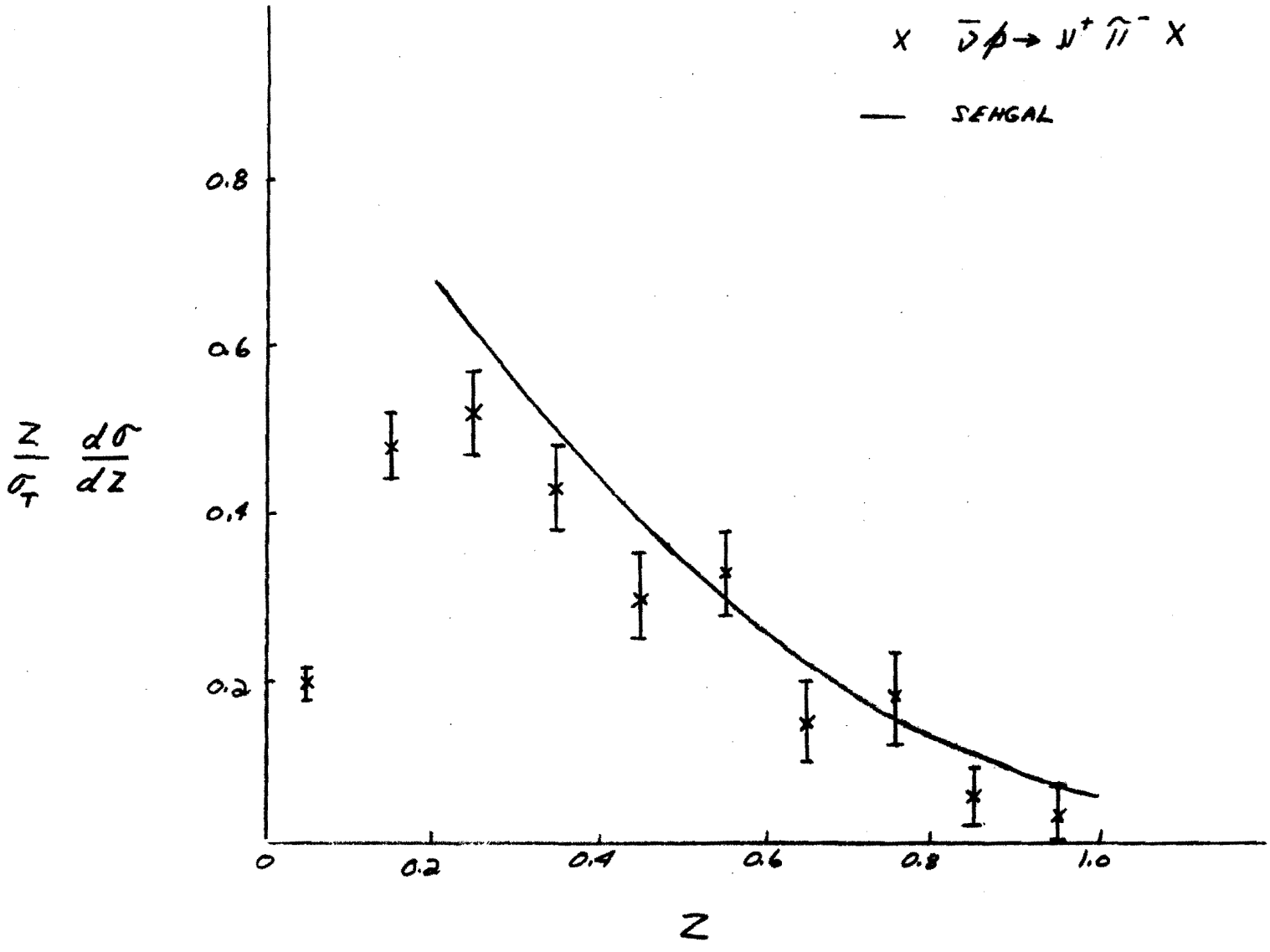
X $\bar{\nu} p \to \mu^+ \pi^- X$
SEHGAL
$\frac{z}{\sigma_T} \frac{d\sigma}{dz}$
0.8
0.6
0.4
0.2
0
0.2
0.4
0.6
0.8
1.0
z

Figure 16

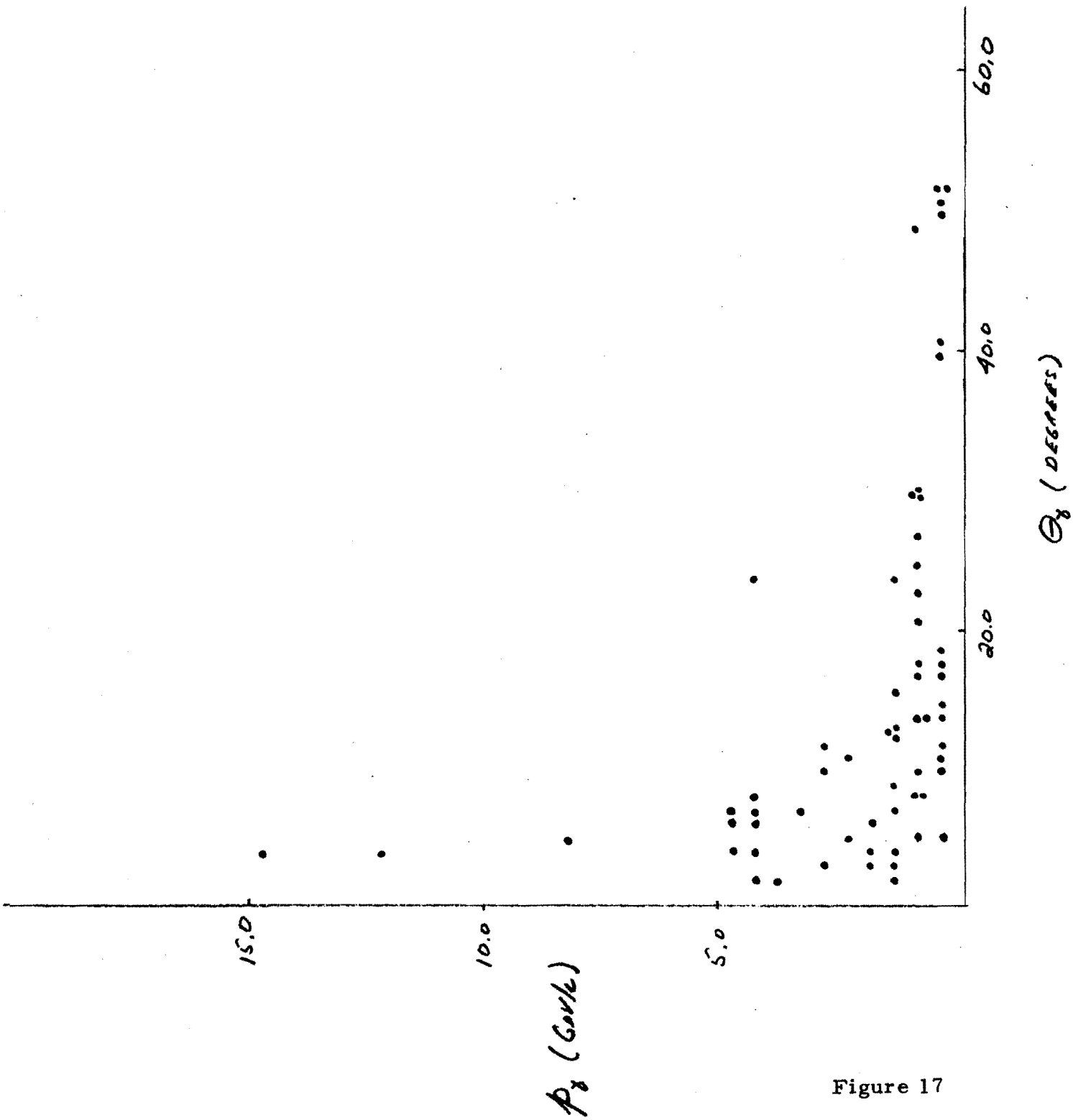

Figure 17

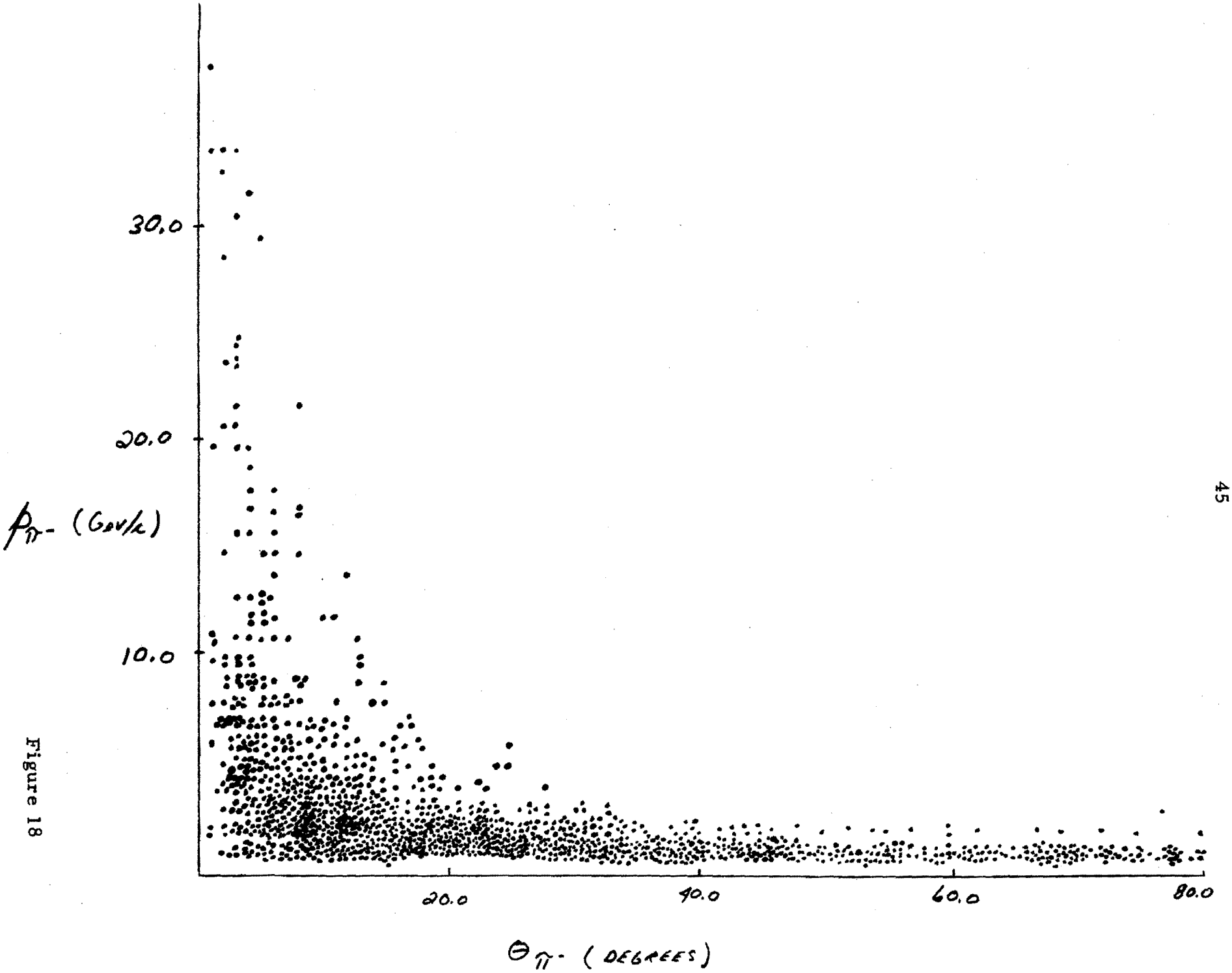

Figure 18

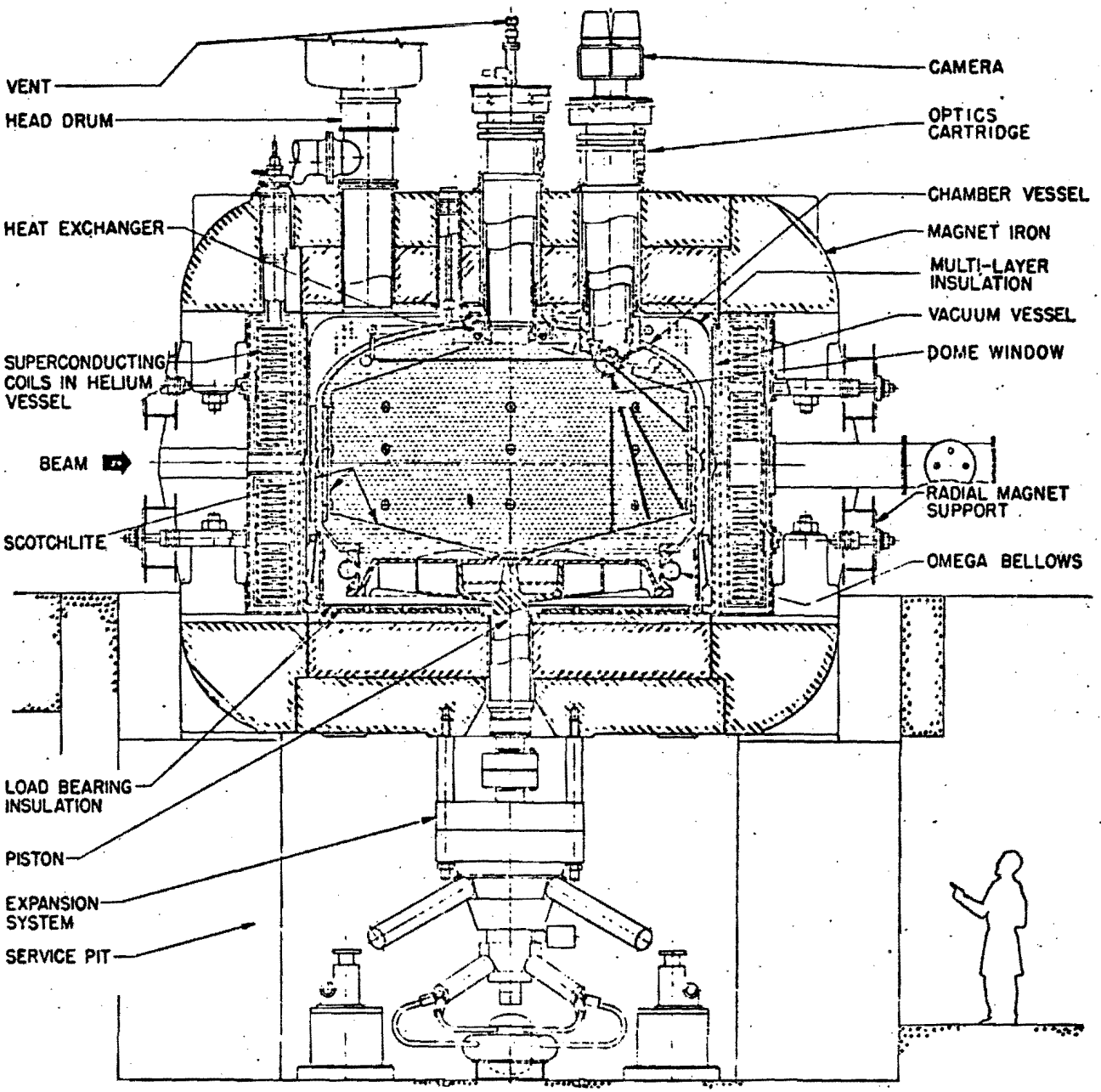
VENT
HEAD DRUM
HEAT EXCHANGER
SUPERCONDUCTING COILS IN HELIUM VESSEL
BEAM
SCOTCHLITE
LOAD BEARING INSULATION
PISTON
EXPANSION SYSTEM
SERVICE PIT
CAMERA
OPTICS CARTRIDGE
CHAMBER VESSEL
MAGNET IRON
MULTI-LAYER INSULATION
VACUUM VESSEL
DOME WINDOW
RADIAL MAGNET SUPPORT
OMEGA BELLOWS

Figure 19

Fermilab Proposal No. 542A

Scientific Spokesman:
D. D. Carmony
Physics Department
Purdue University
W. Lafayette, IN 47907
(317) 749-2961
FTS: 331-7000 Off-Net
Lafayette 749-2961

PROPOSAL TO STUDY $\bar{\nu}p/\bar{\nu}n$ INTERACTIONS IN THE 15-FOOT BUBBLE CHAMBER WITH γ-CONVERTING PLATES

M. Derrick, P. Gregory, L. G. Hyman, K. Jaeger, G. Levman, J. Loos, B. Musgrave, P. Schreiner, J. Schlereth, and R. Singer

Argonne National Laboratory

S. J. Barish, R. Brock, A. Engler, T. Kikuchi, R. Kraemer, F. Messing, B. Stacey, and M. Tabak

Carnegie-Mellon University

V. E. Barnes, T. S. Carman, D. D. Carmony, A. F. Garfinkel, L. Gutay, C. Kennedy, A. T. Laasanen, and L. K. Rangan

Purdue University Group D

December 27, 1977

ABSTRACT

We propose to study antineutrino interactions with protons and neutrons separately, utilizing the 15-foot bubble chamber with the External Muon Identifier (EMI) and the Downstream Plate Converter (DPC) system. The DPC system allows one to study interactions with free nucleons while simultaneously obtaining 65% γ conversion probability. Measurement of the γ energy from π^o decays greatly reduces the systematic errors in the measurement of total hadron energy and momentum, improving the resolution of $d\sigma/dx$ and $d\sigma/dy$ (x and y are the usual leptonic scaling variables) in charged-current interactions with protons and neutrons separately. In addition, we will be able to measure for the first time $d\sigma/du$ [$u = x(1-y)$] for weak neutral-current interactions. We will also identify clean samples of events with zero and one π^o for studies of exclusive final states.

In addition to photon conversion, the DPC will provide ~ 95% efficient electron identification for study of final states with more than one lepton or with an electron accompanied by a strange particle.

CONTENTS

SUMMARY OF REQUEST

We request a wide-band antineutrino exposure of the 15-foot bubble chamber filled with deuterium. The exposure would consist of 7.5×10^{18} protons at 400 GeV incident on the target using the double horn + plug focussing system. Assuming an average intensity of 1.5×10^{13} protons per pulse, we would take 500,000 pictures. We also request that the chamber be equipped with the Downstream Plate Converter (DPC) system and that the improved External Muon Identifier (EMI) with the picket fence be in full operation.

If,for technical reasons, the chamber with the DPC is first filled with H_2, we also request an engineering run in hydrogen.

SUMMARY OF PHYSICS GOALS

The physics discussed in this proposal is primarily that which is made possible or greatly improved by the use of the DPC and free neutron and proton targets. The most important topics we will study are:

(1) The space-time and isospin structure of the weak neutral current.

(2) The origin of μe events seen in several neutrino experiments.

(3) The nature of scaling violations in charged-current interactions.

(4) A detailed probing of the quark-parton structure of the proton and neutron.

(5) Test of the GIM mechanism by studying charmed-particle production by $\bar{\nu}$ with protons and neutrons separately.

STRUCTURE OF THE WEAK NEUTRAL CURRENT

Although existing neutral current data are not in disagreement with the Weinberg model, a direct determination of the space-time and isospin structure of the weak neutral current remains a crucial experimental problem.

A. Analysis of the Inclusive Neutral Current Reaction in Terms of the Scaling Variable u

Any attempt to study the details of the neutral current interaction in the 15-foot bubble chamber requires the improved EMI. This statement is independent of the liquid, the beam, or the plate arrangement used. One expects the EMI to achieve a muon detection efficiency of $\sim$ 95% with quite low hadron punchthrough probability ($< 10^{-4}$). Nearly all the charged current background will be removed using the EMI.

Most reasonable models of weak neutral currents contain four coupling constants which determine the mixing of vector, axial-vector, isoscalar, and isovector components of the current. The most straightforward way of determining these constants is by measuring cross sections from proton and neutron targets separately. This requires the use of deuterium since secondary interactions in heavy target nuclei introduce severe systematic uncertainties which prohibit clear neutron-proton separation. Using isoscalar targets permits measurement of only two relationships among the four coupling constants. In an experiment with free nucleon targets, all four constants can be determined simultaneously by studying the differential cross sections. This can be seen, for example, in the antineutrino $y(= E_{hadron}/E_{neutrino})$ distributions:[1]

$$\frac{d\sigma}{dy}(\bar{\nu}p) = g_L^p(1-y)^2 + g_R^p$$

$$\frac{d\sigma}{dy}(\bar{\nu}n) = g_L^n(1-y)^2 + g_R^n \quad .$$

For a pure vector, isoscalar current, the relation $g_L^p = g_R^p = g_L^n = g_R^n$ holds, while for the Weinberg-Salam model (with $\sin^2\theta_w = 0.23$) $g_L^p = 0.92$, $g_R^p = 0.05$, $g_L^n = 0.48$, $g_R^n = 0.04$. One can measure distributions in the variable $u = x(1-y) = P_H\theta_H^2/2M_p$ which depends only on the variables of the hadronic system. Measurements of the charged hadron momentum with low multiple scattering and low interaction probability will provide a precision measurement of $\vec{P}_H$ (charged). Photon conversion plates will provide ~ 75% of the remaining hadron momentum which would otherwise disappear in neutral mesons. Utilizing the plates, the resolution in u for small u($u < 0.1$) is 0.02 (Fig. 2). With this resolution, the unfolding of the coupling constants will be possible. Without the plates (Fig. 2), the resolution is three times worse. To demonstrate the need for the resolution provided by the plates, we show the theoretical u distributions for several forms of the neutral current in Fig. 3.

It should also be noted that in the case of a D_2 fill, the neutron and proton targets are exposed to precisely the same flux spectrum so that these results will not depend on normalizations or on spectrum calculations as in the case of $\nu, \bar{\nu}$ cross section comparisons.

Because of the shorter nuclear interaction length, the narrow-band experiments proposed in neon cannot measure the hadronic system as well as in deuterium. In heavy neon about 10% of the events are unmeasurable and these, of course, tend to be the high multiplicity, high y events. Furthermore, experiments utilizing heavy nuclei will not be able to distinguish neutron targets from proton targets due to charge exchange and strong interactions in the nucleus.

In summary, it should be possible to do rather detailed measurements of the neutral-current interactions in a light liquid + plates experiment. These measurements off free protons and neutrons cannot be achieved by heavy-liquid bubble chambers or by counters.

B. Measurement of the Cross Section Ratios $R^{\bar{\nu}p} = \sigma^{\bar{\nu}p}_{NC}/\sigma^{\bar{\nu}p}_{CC}$ and $R^{\bar{\nu}n}$

Since neutral current interactions contain an undetectable final state neutrino, even the measurement of the ratio of neutral current to charged-current total cross section R is a difficult experimental task. After eliminating or correcting for neutron-induced background, one must calculate the number of real charged-current events assigned to the neutral current sample; neutral current events which are called charged-current and those lost entirely by imposition of a visible energy requirement, must also be estimated. This requires extensive Monte Carlo studies where one must make assumptions not only about the form of the weak interactions, but about the properties of the final state hadronic system. We have made a first measurement of $R^{\bar{\nu}p}$ with a sample of about 120 neutral current candidates from the initial E-31 runs.[2] Within the framework of the Weinberg-Salam model, our value of $R^{\bar{\nu}p} = 0.42 \pm 0.13$ is consistent with $\sin^2\theta_w \leq 0.6$. Our result and the recently published[3] value for $R^{\nu p} = 0.48 \pm 0.17$ both need to be improved before a sensitive test of most forms of the neutral current can be made, but a V+A isovector neutral current is already disfavored by the data. No measurement of the ratio $R^{\bar{\nu}n}$ has yet been made.

The basic separation of events into the neutral current and charged current channels will be aided by EMI improvements, the horn plug, and the gamma detecting plates. Since the plates substantially improve the measurement of the vector momentum of the hadronic system, the charged-current background in the neutral-current sample will be reduced.

C. Antineutrino-Electron Elastic Scattering ($\bar{\nu}_\mu e^- \rightarrow \bar{\nu}_\mu e^-$)

Antineutrino-electron elastic scattering, $\bar{\nu}_\mu e^- \rightarrow \bar{\nu}_\mu e^-$, is a fundamental reaction in the study of neutral currents. The cross section is, of course, very small. Its minimum value (in the Weinberg model), corresponding to $\sin^2\theta_w = 0.125$, is $\sigma_{min} = (G^2 m_e/8\pi)\ E_{\bar{\nu}}(\text{GeV}) = 1.42 \times 10^{-42}\ E_{\bar{\nu}}\ \text{cm}^2/\text{electron}$. Using a Weinberg angle of $\sin^2\theta_w = 0.26$ leads to small increase of that cross section and an expectation of observing <u>eight</u> events in the proposed experiment. Fig. 4 shows the dependence of the cross section on $\sin^2\theta_w$.

Since the cross section is small, the detection of this reaction has been beset by severe background problems from such things as asymmetric electron-positron pairs from γ conversion, Compton electrons, and the reaction $\nu_e n \rightarrow e^- p$. The background situation in a hydrogen/deuterium bubble chamber with downstream plates is ideal. This is because it is a separated function detector with the hydrogen serving as the target and the plates serving as the electron detector. This allows the neutrino interaction point to be studied in detail, without giving up excellent electron detection efficiency, and so permits a strong rejection of asymmetric electron-positron pairs, Compton electrons, and $\nu_e n \rightarrow e^- p$ events.

The technical difficulties of the experiment can be seen from comparing the results of two CERN experiments. The heavy liquid bubble chamber group[4] (based on three events) obtained $\sigma(\bar{\nu}_\mu e \rightarrow \bar{\nu}_\mu e) = 1.0\ ^{+\ 2.1}_{-\ 0.9} \times 10^{-42}\ E_{\bar{\nu}}\ (\text{GeV})\ \text{cm}^2/\text{electron}$, where the errors are 90% confidence level upper limits. The spark chamber experiment[5] has obtained $\sigma(\bar{\nu}_\mu e^- \rightarrow \bar{\nu}_\mu e^-) = (5.4 \pm 1.7) \times 10^{-42}\ E_{\bar{\nu}}\ (\text{GeV})\ \text{cm}^2/\text{electron}$. If this later measurement is correct, we would see $\sim$ 16 events.

MEASUREMENT OF $d^2\sigma/dydx$ FOR INCLUSIVE CHARGED-CURRENT INTERACTIONS OFF FREE PROTONS AND NEUTRONS

The x and y distributions for charged-current $\bar{\nu}$ interactions off protons and neutrons are of fundamental importance. The double differential distribution has not been studied at high energies because of limited statistics. Although the x- and y-variables can be measured with some precision in a bare bubble chamber, a (statistically valid) correction has to be made for the roughly 1/3 of the hadron energy carried away by neutrals. Since the plates convert 75% of the energy carried away by π^0's, the determination of energy and the scaling variables x and y is much improved as can be seen in Figs. 5, 6 and 7. Thus a large deuterium exposure with the proposed plate array is needed to measure the quark content of the proton and neutron, to study scaling violations, and examine questions such as quark fragmentation.

A. The Charged-Current y Distribution

One topic which has been discussed extensively is the high energy behavior of antineutrino interactions, in particular the question of the so-called high-y anomaly. The differential distribution dN/dy, where N is the number of charged current events, can be written in the context of the quark parton model (QPM):

$$dN/dy \propto (1 - y + \tfrac{1}{2}y^2) - By(1 - \tfrac{1}{2}y) \quad , \qquad (1)$$

where B is related to the quark-antiquark content of the nucleon, $B = (Q - \bar{Q})/(Q + \bar{Q})$. B is expected to be about 0.8 - 0.9 on theoretical grounds and experiments at energies up to 30 GeV have indeed found compatible values of B. The HPWF experiment,[6] however, reported a B value of 0.41 ± 0.13 for antineutrino interactions at about 70 GeV. Our present value of B for $\bar{\nu}p$ interactions is 0.84 ± 0.13 at an average energy of 55 GeV (see Fig. 8). We expect to report on the completed E-31 data sample early in 1978 (a five-fold increase in data).

In the deuterium experiment, we will compare $B^{\bar{\nu}p}$ with $B^{\bar{\nu}n}$ as a function of energy.

B. The Charged Current x Distributions

Since the antiquark content of the proton is small and limited to x values less than $\sim$ 0.2, the x-distributions for $\bar{\nu}p$ and $\bar{\nu}n$ interactions predominantly measure the u(x) and d(x) distributions, respectively.

Fig. 9 shows the ratio of the νp and $\bar{\nu}p$ x distributions (from E-31 and E-45) as a function of x. For $x > 0.2$, this quantity also measures the ratio (d/u) of the down to the up quarks inside the proton. Also shown in Fig. 9 is the appropriate combination of ep and ed x distributions, which again measures the d/u ratio for $x \geq 0.2$. The shapes of the data agree and one sees the u quark leading at the higher x values. The curves represent the normalized functions of Field and Feynman[7] and since they take explicit account of sea quarks, the agreement is quite good at all values of x.

By using deuterium as a target, it is possible in <u>one</u> experiment to measure the absolute value (not just the shape) of the ratio of the down-to-up quark distributions as a function of x. For x values greater than $\sim$ 0.2 (where the sea contributions are small), one has

$$R = \frac{d(x)}{u(x)} = \left(\frac{d\sigma}{dx}\right)_{\bar{\nu}n} / \left(\frac{d\sigma}{dx}\right)_{\bar{\nu}p} \quad . \tag{2}$$

Many theorists regard the large x behavior of this ratio to be of high importance, but are not able to make unique predictions. For example, R. Feynman[8] predicts $R \to 0$ as $x \to 1$, while G. Farrar[9] predicts $R \to 0.2$; precise measurement in the range $x > 0.60$ would be of great value in resolving this question. In Feynman's model, there would be $\sim$ 50 $\bar{\nu}n$ events and $\sim$ 600 $\bar{\nu}p$ events with $x \geq 0.6$ in 500K deuterium pictures. The resolution in x at large x is substantially improved by the presence of the γ-converting plates.

Recent work on quark recombination in the fragmentation region at low p_T in pp collisions, by Duke and Taylor,[10] based on the model of Das and Hwa,[11] relates the ratio of produced π^-/π^+ to the ratio of the down-to-up quark distribution functions, d(x)/u(x) as measured in lepton interactions. The two ratios exhibit a striking similarity for large x, as noted by Ochs[12] and a value of R = 0.20 as $x \to 1.0$ is found. Duke and Taylor find that for single particle production in pp collisions, the quark recombination process is dominant compared to quark fragmentation and that this then implies a much larger effective sea quark distribution than is determined from lepton interactions. A detailed study of the hadronic system produced in $\bar{\nu}$ interactions, in the context of the quark recombination and fragmentation models, may yield important insights.

C. Checks of Callan-Gross Relationship and of Scaling

Additional data, especially for the antineutrino interaction, are needed to check experimentally the Callan-Gross relation,[13] i.e. that the terms linear and quadratic in y are related as stated in Eq. (1). Even assuming that the y-distribution can be parameterized in terms of a single B-parameter, one wants to examine the x-dependence of B. Recalling that $B(x) = (Q - \bar{Q})/(Q + \bar{Q})$ measures the relative antiquark content of the struck nucleon, one expects that B is small at small x. We propose to measure $B(x)^{\bar{\nu}p}$ and $B(x)^{\bar{\nu}n}$ and compare with lower energy data.

D. Quark Fragmentation

Next to observing quarks directly, one of the more interesting studies of them is to see how they radiate hadrons after being struck in leptonic collisions.

The deuterium bubble chamber can measure all final state charged

hadrons and with γ-detecting plates, most of the π^0's as well. This allows one to analyze the quark fragmentation in detail.[14] The parton fragmentation hypothesis is the statement that if a hadron (with four-momentum h) is a fragment of a parton, then its momentum distribution will depend only on the invariant $Z = (h \cdot p)/(q \cdot p)$ where p is the initial four-momentum of the target nucleon and q is the four-momentum absorbed by the parton in the collision. In the laboratory, the variable Z reduces (e.g. for a pion fragment) to $E_\pi/(E_\nu - E_\mu)$, the ratio of the energy of the pion to the total energy transfer. Thus one regards the Z distribution as a measure of the probability distribution for a fragmenting quark to produce a hadron of fractional energy Z. From this it follows that in the current fragmentation region (large Z), the Z distribution should scale. Sehgal predicted from electroproduction measurements, the absolute distribution of $(Z/\sigma_T)\, d\sigma/dZ$ for pion production by antineutrinos. Fig. 10 shows his prediction and our measurements. The agreement is quite good for $Z \gtrsim 0.3$. With gamma-converting plates, we will be able to measure the fragmentation function $D_d^{\pi^0}$ and improve the resolution in Z for charged pions.

Finally, if these relations continue to work well with improved data, one can, as discussed by Sehgal,[15] study the Z distributions in neutral current interactions.

DILEPTONS AND THE SEARCH FOR CHARMED PARTICLE PRODUCTION BY ANTINEUTRINOS

Electronic experiments[17, 18] have observed dimuon production by neutrinos at about the one percent level. These experiments have found a similar rate for production by antineutrinos. Bubble chamber experiments[19] at FNAL have observed μ-e production by neutrinos at about the 0.6% level, and by antineutrinos at the 0.2% level.

One possible explanation of dilepton production is charm particle production. While neutrinos can produce charmed particles from the valence quarks, the process is suppressed by $\sin^2\theta_c$ which is $\sim$ 0.05. The production of charmed mesons by antineutrinos is Cabibbo allowed but must occur on anti-strange quarks which should occur at the few percent level in the nucleon sea. A measurement of the relative amount of charm production in neutrino and antineutrino interactions checks these concepts.

Since the dominant decay of charmed particles is expected to be into hadrons, it is important to search for them in invariant mass distributions, making use of the excellent effective mass resolution of the deuterium bubble chamber. The γ plates are likely to be vital in finding the π^o decay products of these decays and so in completely specifying the hadronic final state (Appendix II).

With the addition of plates and use of the improved External Muon Identifier, the deuterium filled bubble chamber will become a highly competitive device for studying semileptonic decays of charmed particles. Electrons with momentum less than 0.5 GeV/c will be trapped in the bubble chamber and clearly recognized. Asymmetric Dalitz decays are a principal source of potential background and are much more easily recognized in a deuterium bubble chamber with its low density and long radiation length. The plates are necessary for recognizing higher momentum electrons. Of the electrons which pass through the plate array, 95% will be recognized as electrons; hadron misidentification is a very minor problem (see Appendix I).

$\Delta S = 1$ REACTIONS

The study of the two-body strangeness-changing reactions over a wide range of energy and momentum transfer will extend our understanding of the weak interaction. For reactions involving hyperons from the baryon octet

$$\bar{\nu} p \to \mu^+ \Lambda^o \quad (\Lambda^o \to p\pi^-) \qquad \text{(50 events)} \qquad (3)$$

$$\bar{\nu} p \to \mu^+ \Sigma^o \quad (\Sigma^o \to \Lambda^o \gamma) \qquad \text{(14 events)} \qquad (4)$$

$$\bar{\nu} n \to \mu^+ \Sigma^- \qquad \text{(38 events)} \quad , \qquad (5)$$

the predicted rates in the Cabibbo model[16] are indicated. Of equal interest is a study of the reaction

$$\bar{\nu} n \to \mu^+ \Sigma^*(1385)^- \quad (\Sigma^* \to \Lambda^o \pi^-) \qquad (6)$$

and comparing its rate to that of

$$\bar{\nu} p \to \mu^+ \Delta^o(1238) \quad (\Delta^o \to p\pi^-) \quad . \qquad (7)$$

Again, it would form a test of the Cabibbo model, and the fact that the Σ^* and Δ^o are in a decuplet means that no F/D ratio is involved.

The study of these reactions can, of course, only be carried out in a deuterium bubble chamber although even here it will be difficult. In neon, strange particles can be readily produced or absorbed in the nucleus so as to make such measurements highly uncertain. The chief advantage of the plates in the study of these reactions will be to veto events with additional π^o's in the final state and so validate the selection techniques.

The rate for inclusive reactions such as

$$\bar{\nu} p \to \mu^+ \Lambda^o X^o$$
$$\bar{\nu} p \to \mu^+ \overline{K}^o B^o$$
$$\bar{\nu} n \to \mu^+ \overline{K}^o B^- \quad ,$$

where $X^o(B^o, B^-)$ is a nonstrange mesonic (baryonic) system, will presumably be something like 5% ($\sim \sin^2\theta_c$) of the total rate. This will mean detecting approximately 400 such events. The plates system will be invaluable in detecting the π^o component of $X^o(B^o, B^-)$. To the extent that they allow a

complete characterization of the final state, they will enable one to obtain a sample uncontaminated by associated production. Our ability to reconstruct π^{o}'s is discussed in Appendix II.

TIME SCALE OF THE EXPERIMENT

If all of our pictures were obtained in one run, all of the scanning and measuring of the film will be completed within 18 months. Since we already have considerable experience with 15-foot chamber data analysis, physics results will be obtained very quickly.

We note that the scanning and measuring of our recent 150,000-picture E-31 exposure will be completed by April 1978.

REQUESTED PLATE ARRANGEMENT

We propose to utilize a set of four closely spaced plates in the downstream region of the bubble chamber as shown in Fig. 1. The configuration discussed by D. Theriot and D. Carmony at the October and November 1977 PAC meetings is nearly identical to our original design except that the plates are steel rather than tantalum. Since the same number of radiation lengths (3) is used, the only physics price paid is that there are somewhat more nuclear interactions by secondaries in the plates. The ability to rapidly fabricate and test steel plates makes this choice reasonable.

The plates convert 90% of the incident γ's. We find that 65% of the gammas produced in the fiducial volume upstream of the plates are converted and that this represents 75% of the energy carried off by π^{o}'s. Fig. 11 shows (E-31 data) our observed laboratory momentum-angle scatter plot

of gammas that convert in the hydrogen. Fig. 12 is a similar plot for the observed π^{-}. These plots show that energetic gammas have a high

probability of intercepting the plates.

APPENDIX I

Electron Identification with the Proposed Plate Array

We expect that about 40-50% of all electrons produced in $\bar{\nu}_\mu$ events will penetrate the downstream plate array or be trapped by the magnetic field. Above 1 GeV/c, an electron which goes through the plates can be identified 95% of the time and the probability that a pion will fake an electron is less than 1/7000 at 1.6 GeV and falls to 1/30,000 at 3 GeV. This plate technique has been used successfully at SLAC.

Recent experience with heavy metal plates mounted in the SLAC 40-inch bubble chamber proves that this technique provides excellent $e^{\pm}$ signatures and excellent $\pi^{\pm}$ rejection.* The plate system used at SLAC for BC-65, described below, has approximately the same $e^{\pm}$ detection properties as the proposed plate system for the Fermilab 15-foot bubble chamber. The conclusions of the BC-65 experimenters are (a) at 1.6 GeV/c approximately one incident $\pi^{\pm}$ in 20,000 causes a fake $e^{\pm}$ shower, (b) at 3.1 GeV/c approximately one incident $\pi^{\pm}$ in 100,000 causes a fake $e^{\pm}$ shower, and (c) a good signature for true $e^{\pm}$ tracks occurs $(94 \pm 1)\%$ of the time above 1 GeV/c.

A brief description of the SLAC plate system is now given. The system has three tantalum plates, each 1.0 radiation length thick, and separated from one another by approximately 9 cm. The magnetic field in the chamber is 26 kG. Calibration runs were taken in order to study the $e^{\pm}$ identification and $\pi^{\pm}$ rejection properties of this system. Fig. 13 shows two typical electromagnetic showers caused by e^{+} particles incident at 1.6 GeV/c. The members of these showers exhibit the following characteristics: (a) multiplication in

*Duke-SLAC-Imperial College Collaboration, Washington APS Meeting, April 1977 and to be published.

numbers from plate-to-plate, (b) small transverse momenta relative to the incident particle direction, (c) large energy losses when penetrating a plate, and (d) emission of bremsstrahlung photons near 0°, in the straight-ahead direction. Fig. 14 shows a typical π interaction. The hadron-induced "showers" have quite different characteristics from those of the electromagnetic showers: (a) particles are usually produced at wide angles or at high transverse momenta, (b) "shower" members usually penetrate through downstream plates without significant energy loss, and (c) often some tracks have high density.

Below we give a brief explanation of the cuts used in BC-65 to select $e^{\pm}$ showers and to reject $\pi^{\pm}$ "showers".

Based on the experience of BC-65 at SLAC, we conclude that the proposed plate system for the 15-foot chamber (four steel plates, each 0.72 radiation lengths thick) will provide $\pi^{\pm}$ rejection factors of approximately 7000 at 1.6 GeV/c and 30,000 at 3.1 GeV/c, while identifying $\sim 95\%$ of the $e^{\pm}$ particles incident on the plates above 1 GeV/c. We have assumed that the $\pi^{\pm}$ rejection of the steel plates is three times poorer than for tantalum because of the lsss favorable ratio of radiation length to nuclear absorption length. Incidentally, we note that in order to achieve good $\pi^{\pm}$ rejection, it is necessary to have three or more plates. The downstream plates are needed to identify penetrating hadrons and wide-angle gamma rays associated with $\pi^{\pm}$ "showers". We also note that the $\pi^{\pm}$ rejection improves as the incident momentum is increased. This fact reflects the energy dependence of the pion charge-exchange cross section.

We give here a brief summary of the variables and cuts used by BC-65 to reject the $\pi^{\pm}$ "showers".

Definitions:

(a) E_{vis} = visible energy in the shower.

(b) $P_T(e)_{max}$ = maximum transverse momentum of any charged track in the shower.

(c) $P_T(\gamma)_{max}$ = maximum visible transverse momentum of any associated gamma ray.

Cuts used (if a "shower" fails any of these, it is considered to be a pion).

(1) No $e^{\pm}$ above 10 GeV produced at greater than 90^{o} at the first plate.

(2) E_{vis} (at first plate) must exceed 20 MeV.

(3) E_{vis} in shower must exceed 0.2 of the incident energy.

(4) $P_T(e)_{max}$ must be less than 30 MeV/c.

(5) $P_T(\gamma)_{max}$ must be less than 20 MeV/c.

APPENDIX II

Monte-Carlo Determination of the Ability to Reconstruct the π^o from $\gamma\gamma$ Events

We have obtained an estimate for π^o mass reconstruction from converted e^+e^- pairs using a Monte Carlo simulation based on the assumption that the π^o momentum and multiplicity distributions are equal to the π^- distributions observed in E-31. Photons resulting from the π^o decays were converted in the plates and the invariant mass was calculated from all possible photon pairs. We used our predicted uncertainty in γ-ray energies of about 30% and included measuring error uncertainties for the electrons. Using this simulation, the $\gamma\gamma$ effective mass is shown for all $\gamma\gamma$ combinations in Fig. 15(a) and for the correct $\gamma\gamma$ pairings in Fig. 15(b). The signal-to-noise ratio when all $\gamma\gamma$ combinations are made is about 1:1 where the noise comes from wrong pairings. The correct combinations reproduce the π^o peak with a FWHM of $\sim$ 80 MeV. If we restrict ourselves to those events with two converted gammas (Fig. 16), we note that they are primarily from single π^o events and that much of the multineutral pion wrong combination background (shown shaded) can be removed by a suitable mass cut. The above estimates are derived solely from the direction and energy of the converted γ-rays. We expect to be able to improve on this by using the kinematics of the production vertex.

References

1. J. J. Sakurai, Erice Conference 1976, UCLA/76/TEP/21.
2. M. Derrick et al., Strength of the Antineutrino Neutral Current, Physical Review (to be published).
3. F. Harris et al., Phys. Rev. Letters 39, 437 (1977).
4. J. Blietschan et al., Nucl. Phys. B114, 1891 (1976).
5. F. Bobisut et al., in Neutrino Conference, Aachen 1976, p. 223.
6. A. Benvenuti et al., Phys. Rev. Letters 36, 1478 (1976).
7. R. D. Field and R. P. Feynman, Phys. Rev. D15, 2590 (1977).
8. R. Feynman, Photon-Hadron Interactions, W. A. Benjamin (1972).
9. G. R. Farrar, private communication.
10. D. W. Duke and Frank Taylor, Fermilab-PUB-77/95-THY (October 1977).
11. K. P. Das and R. C. Hwa, Phys. Letters 68B, 459 (1977).
12. W. Ochs, Nucl. Phys. B118, 397 (1977).
13. C. G. Callan and D. J. Gross, Phys. Rev. Letters 22, 156 (1969).
14. L. M. Sehgal, Nucl. Phys. B90, 471 (1975).
15. J. Cleymans and L. M. Sehgal, Nucl. Phys. B74, 285 (1974).
16. Cabibbo and Chilton, Phys. Rev. 137B, 1628 (1965) and Eichten et al., Phys. Letters 40B, 593 (1972).
17. B. Aubert et al., Proc. XVII Conference on High Energy Physics (London) 1974. A. Benvenuti et al., Phys. Rev. Letters 34, 419 and 597 (1975).
18. B. Barish et al., Phys. Rev. Letters 36, 939 (1976).
19. J. VonKrogh et al., Phys. Rev. Letters 36, 410 (1976), J. VonKrogh, Proc. Madison Conference (April 1976), C. Baltay, 1976 DPF Meeting at Brookhaven.

Table I: Total Events ($\bar{\nu}$d) (for 500,000 pictures based on measured event rates from E-31 and 1.5×10^{13} ppp and 12 m^3 fiducial volume)

		Events
A.	Charged Currents - Inclusive Reactions	
	Total $\bar{\nu}_\mu$ p Charged Current (CC) Events	8,000
	Total $\bar{\nu}_\mu$ n CC Events	4,000
	Total $\bar{\nu}_\mu$ CC Events	12,000
	Total $\bar{\nu}_\mu$ CC Events with $E_{\bar{\nu}} > 30$ GeV	6,000
	Total $\bar{\nu}_e$ CC Events	~ 100
B.	Neutral Currents - Inclusive Reactions (Assuming R = 0.40)	
	$\bar{\nu}p + \bar{\nu}n$	4,800

Figure Captions

Fig. 1 Side view of the 15-foot chamber showing proposed downstream plate arrangement.

Fig. 2 Histogram of the uncertainty (du) in the scaling variable u for $\bar{\nu}$ neutral currents (a) without the plates, (b) with the plates. Shown shaded in (b) are the events with $u < 0.1$.

Fig. 3 The u distributions for the $\bar{\nu}$ neutral current interactions for the cases of V+A, V-A, and Weinberg-Salam with $\sin^2\theta_w = 0.3$.

Fig. 4 Neutrino and antineutrino-electron elastic cross sections as a function of $\sin^2\theta_w$.

Fig. 5 The expected resolution in the incident antineutrino energy with and without downstream plates for charged-current events.

Fig. 6 The expected resolution Δx in x for charged-current events using the downstream plates. Fig. (a) is Δx for all x; Fig. (b) is Δx as a function of x.

Fig. 7 The expected resolution Δy in y for charged-current events using the downstream plates. Fig. (a) is Δy for all y; Fig. (b) is Δy as a function of y.

Fig. 8 Measured y distribution for $\bar{\nu} p \rightarrow \mu^+$ interactions.

Fig. 9 Measurements (E-31 and E-45 data) of the ratio of down-to-up quarks as a function of the scaling variable x. The data is compared with electroproduction data from SLAC and a prediction of Field and Feynman (see text).

Fig. 10 The Z distribution for inclusive π^- production by antineutrinos. (Data from E-31.)

Fig. 11 The laboratory momentum versus scattering angle for observed gammas in E-31.

Fig. 12 The laboratory momentum versus scattering angle for observed negative pions in E-31.

Fig. 13 Photograph showing electrons penetrating the SLAC thin plate array.

Fig. 14 Photograph showing a pion penetrating the SLAC thin plate array.

Fig. 15 A Monte Carlo calculation of the $\gamma\gamma$ effective mass of all observed multigamma events using all possible combinations. The inset shows the effective mass of the correct pairings.

Fig. 16 A Monte Carlo calculation of the $\gamma\gamma$ effective mass for all events with two visible gammas. The events shown shaded are wrong combinations from multipion events.

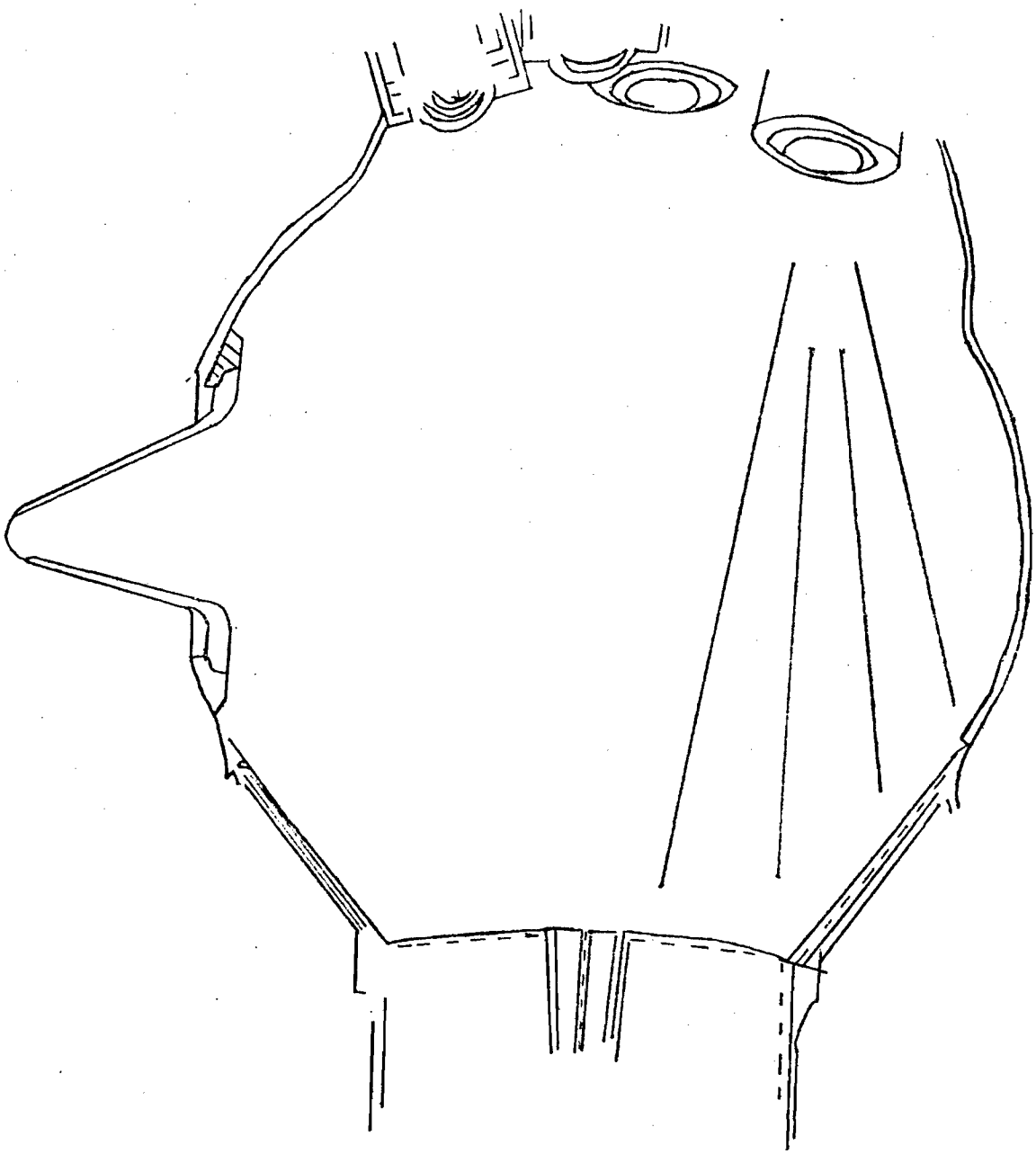

Figure 1

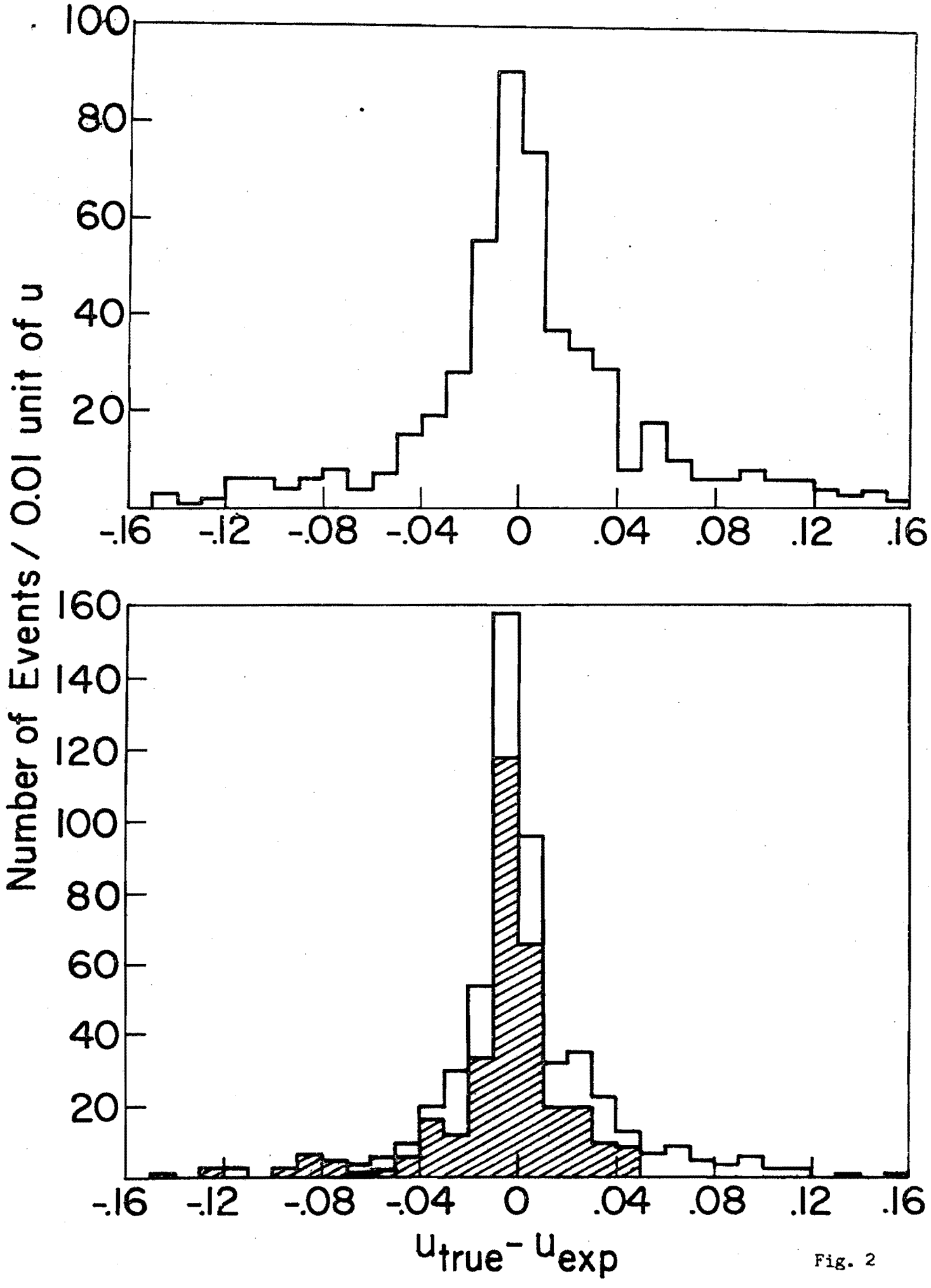
Number of Events / 0.01 unit of u
100
80
60
40
20
-.16
-.12
-.08
-.04
0
.04
.08
.12
.16
160
140
120
100
80
60
40
20
$u_{true} - u_{exp}$

Fig. 2

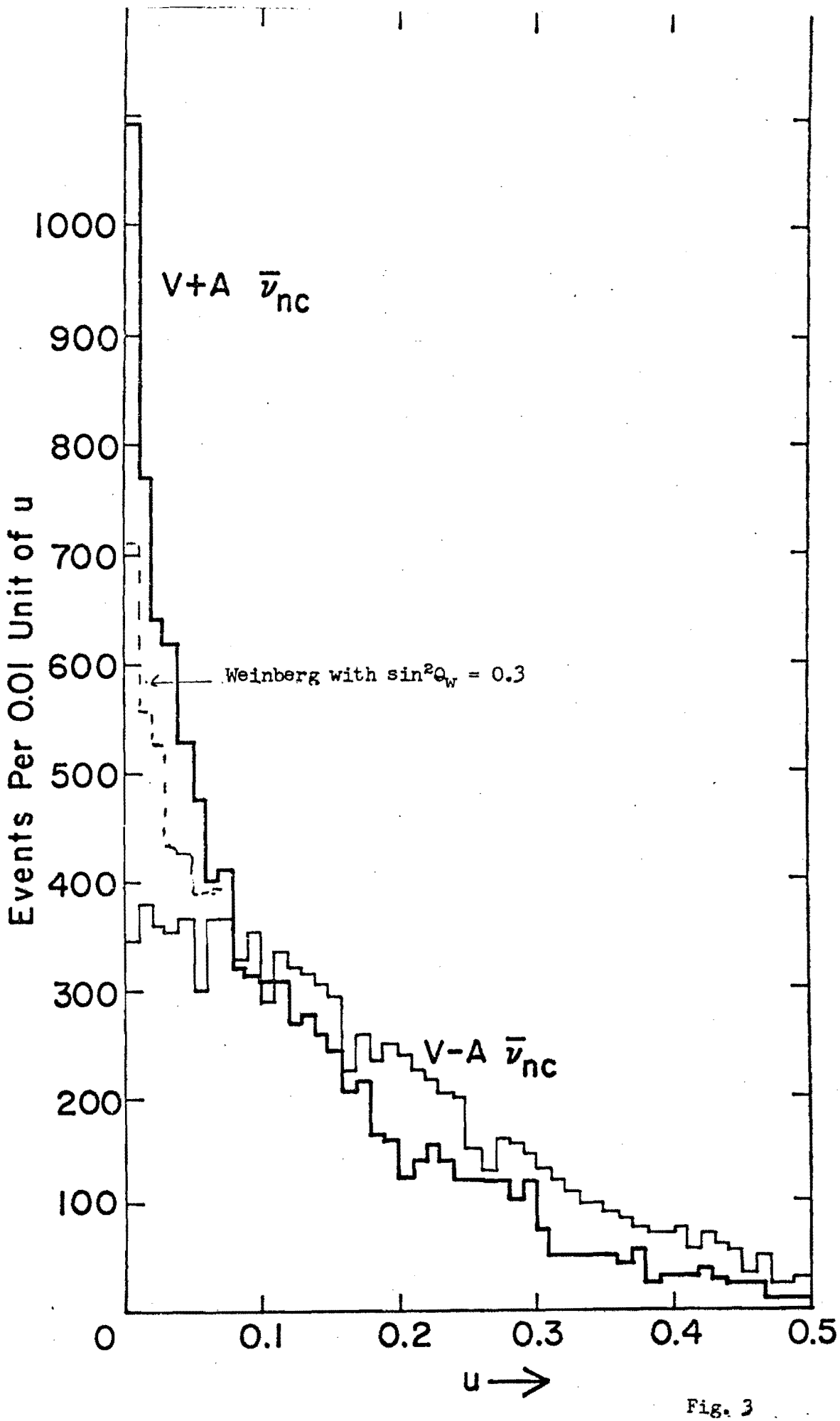
V+A $\bar{\nu}_{nc}$
V-A $\bar{\nu}_{nc}$
Weinberg with $\sin^2\theta_W = 0.3$
Events Per 0.01 Unit of u
u
1000
900
800
700
600
500
400
300
200
100
0
0.1
0.2
0.3
0.4
0.5

Fig. 3

Variation with $\sin^2 \theta_W$ of cross-sections
for the different ν-e processes.

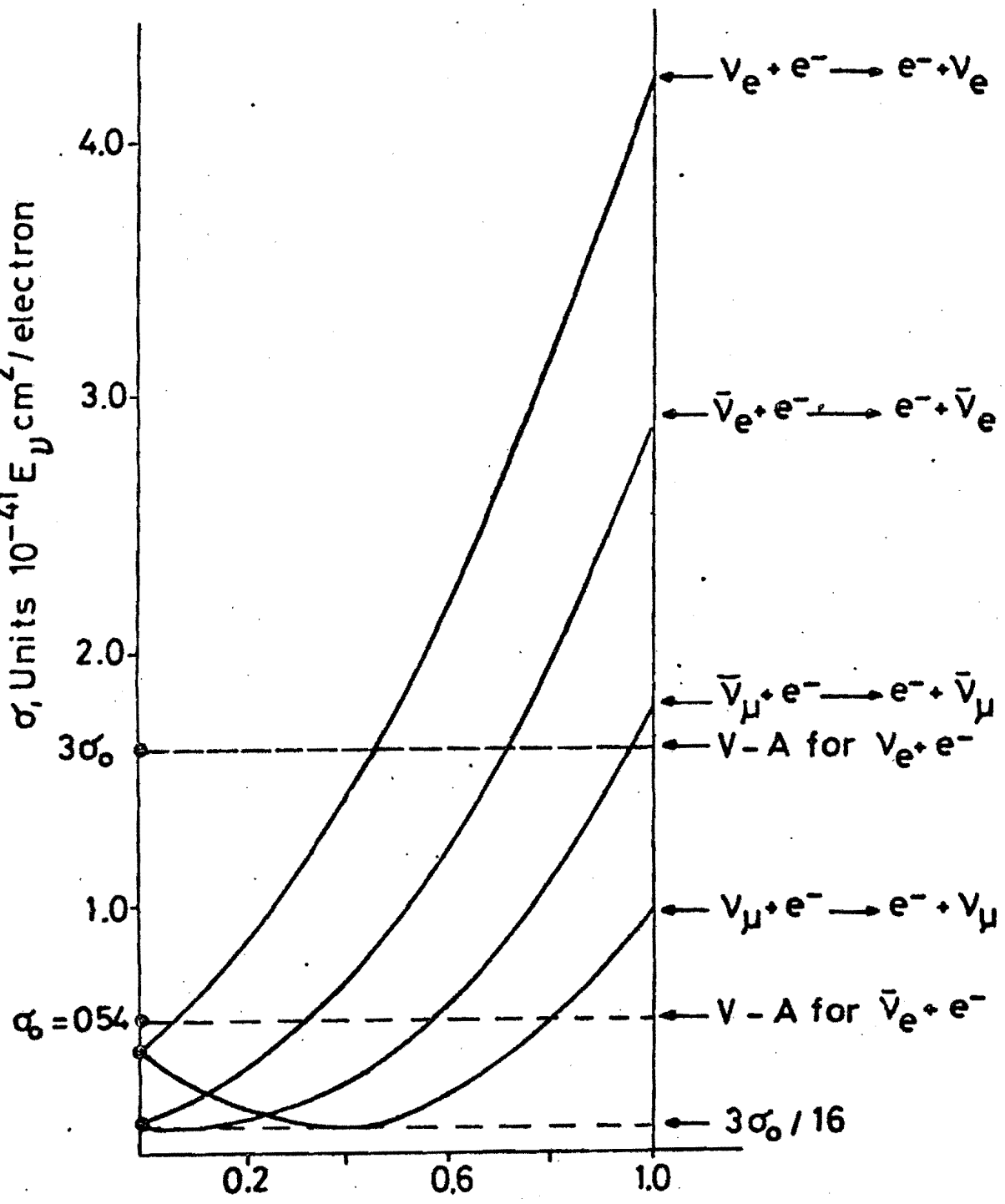

Figure 4

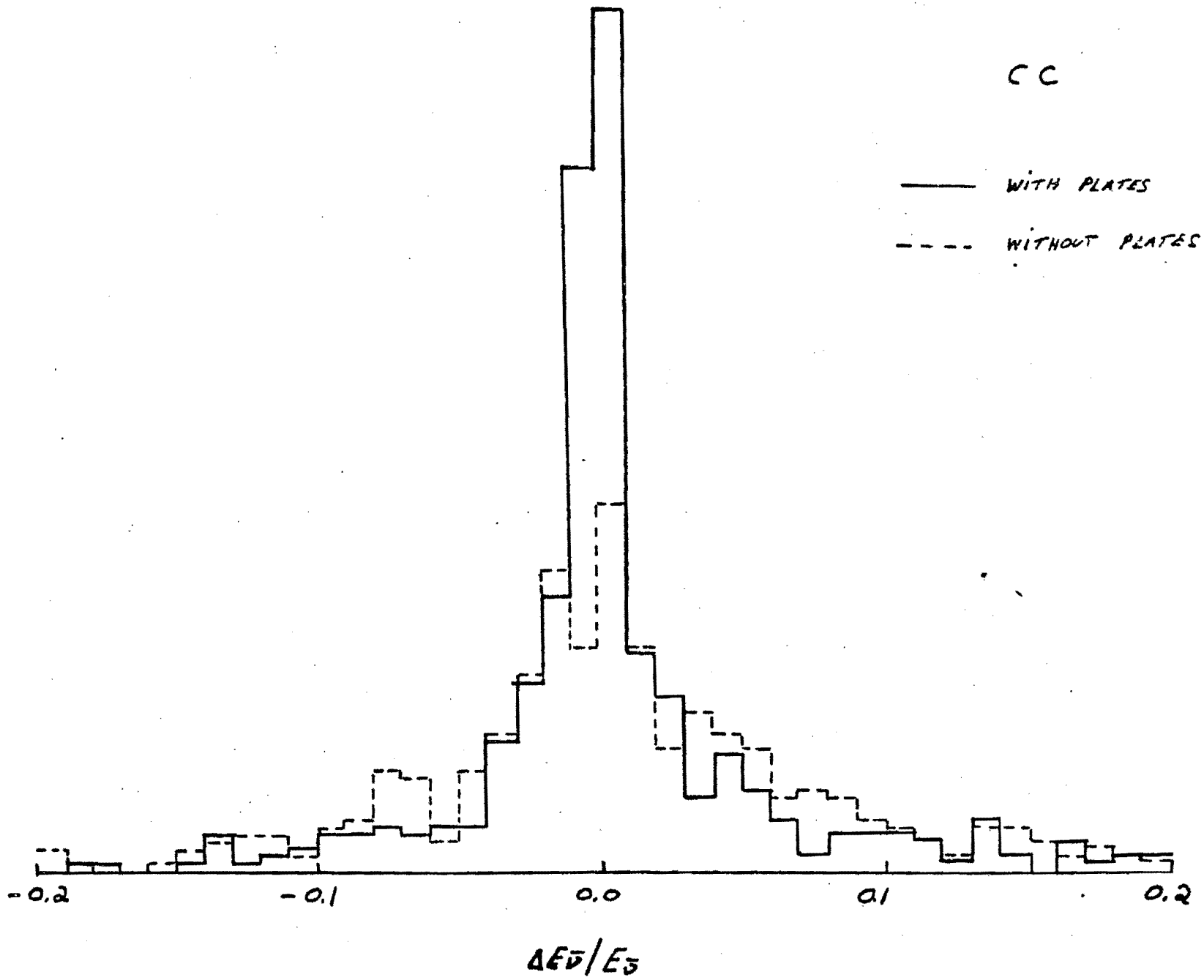

Figure 5

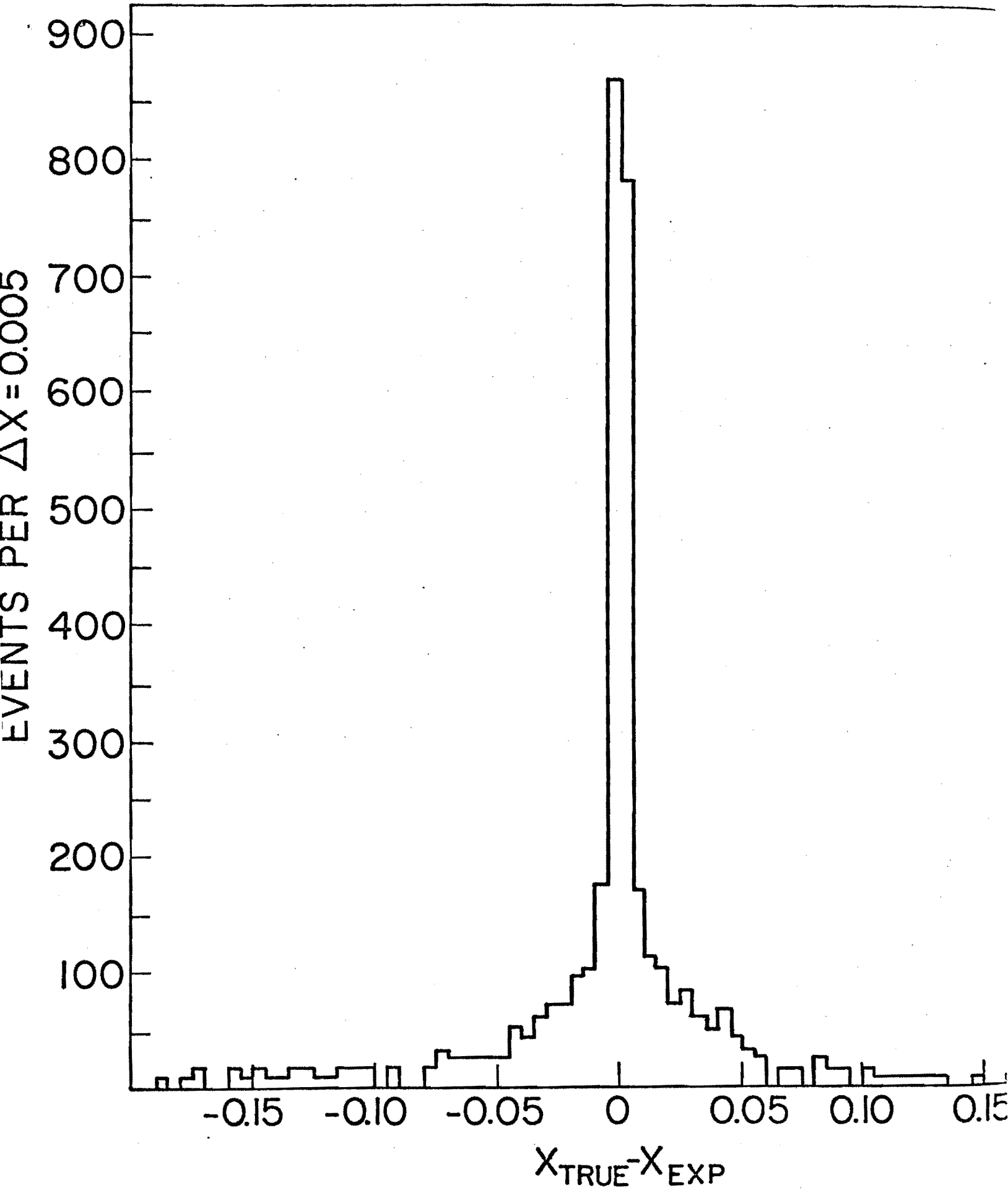
900
800
700
600
500
400
300
200
100
EVENTS PER ΔX = 0.005
-0.15
-0.10
-0.05
0
0.05
0.10
0.15
X_TRUE - X_EXP

Fig. 6a

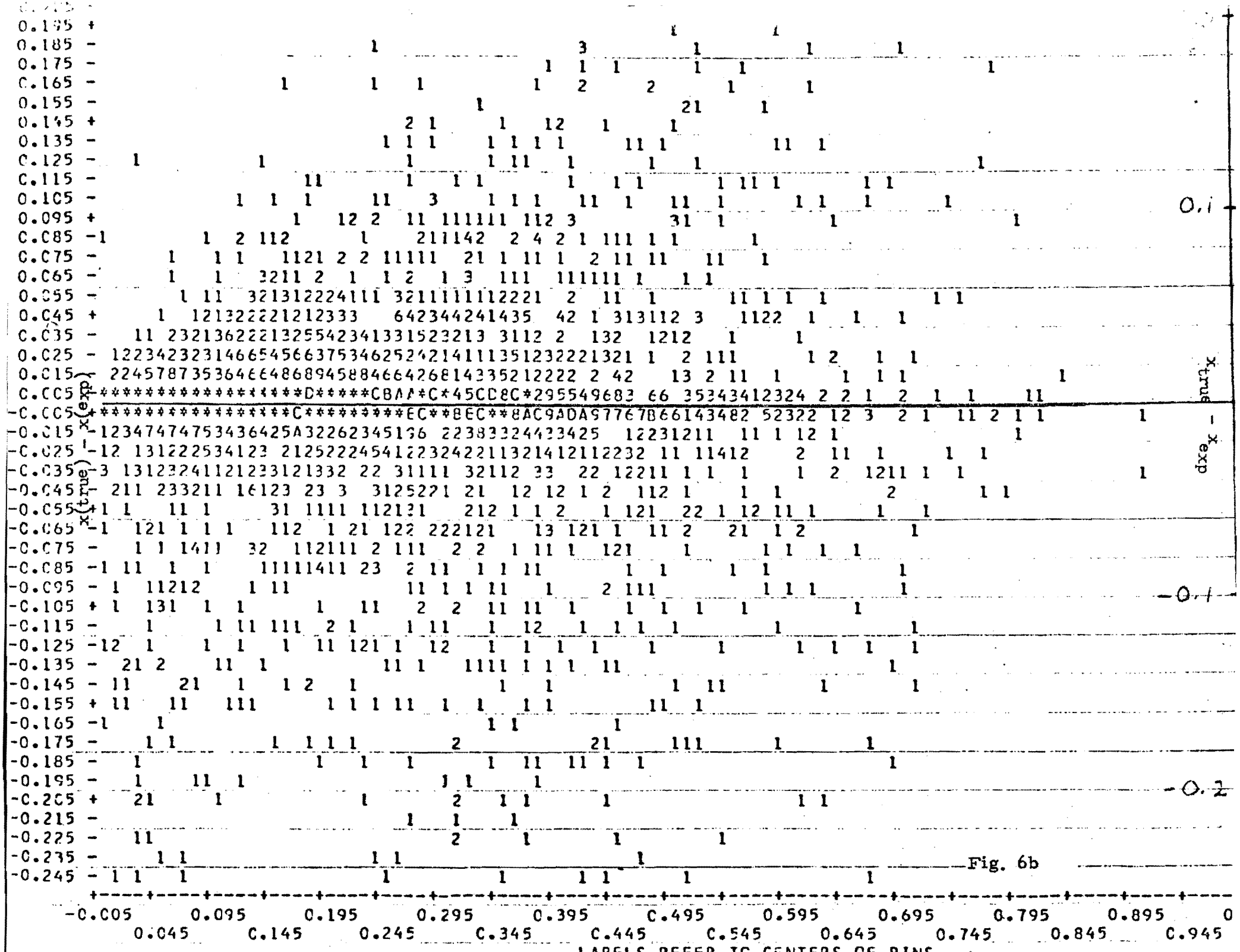

Fig. 6b

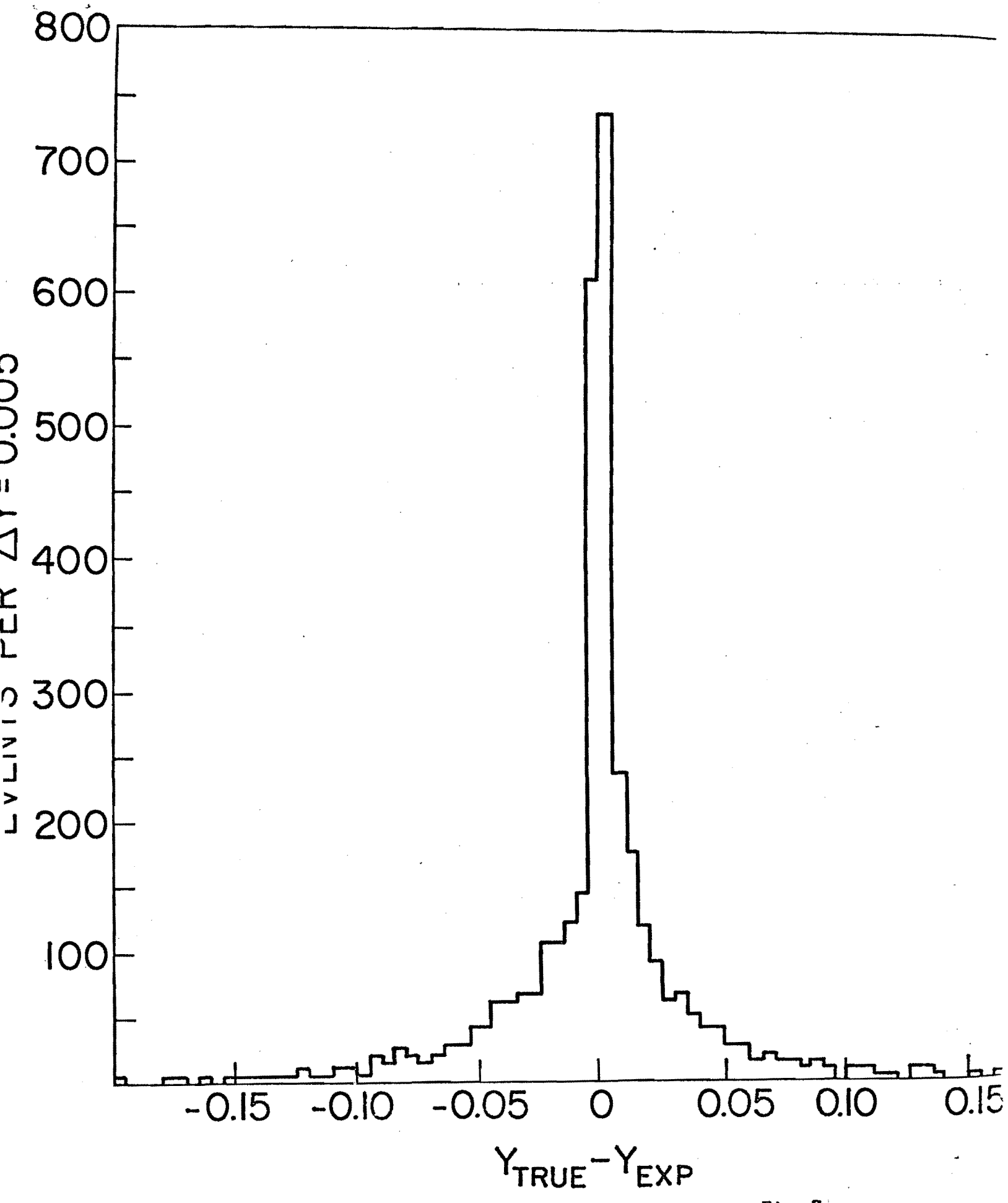
800
700
600
500
400
300
200
100
EVENTS PER ΔY = 0.005
-0.15
-0.10
-0.05
0
0.05
0.10
0.15
$Y_{TRUE} - Y_{EXP}$

Fig. 7a

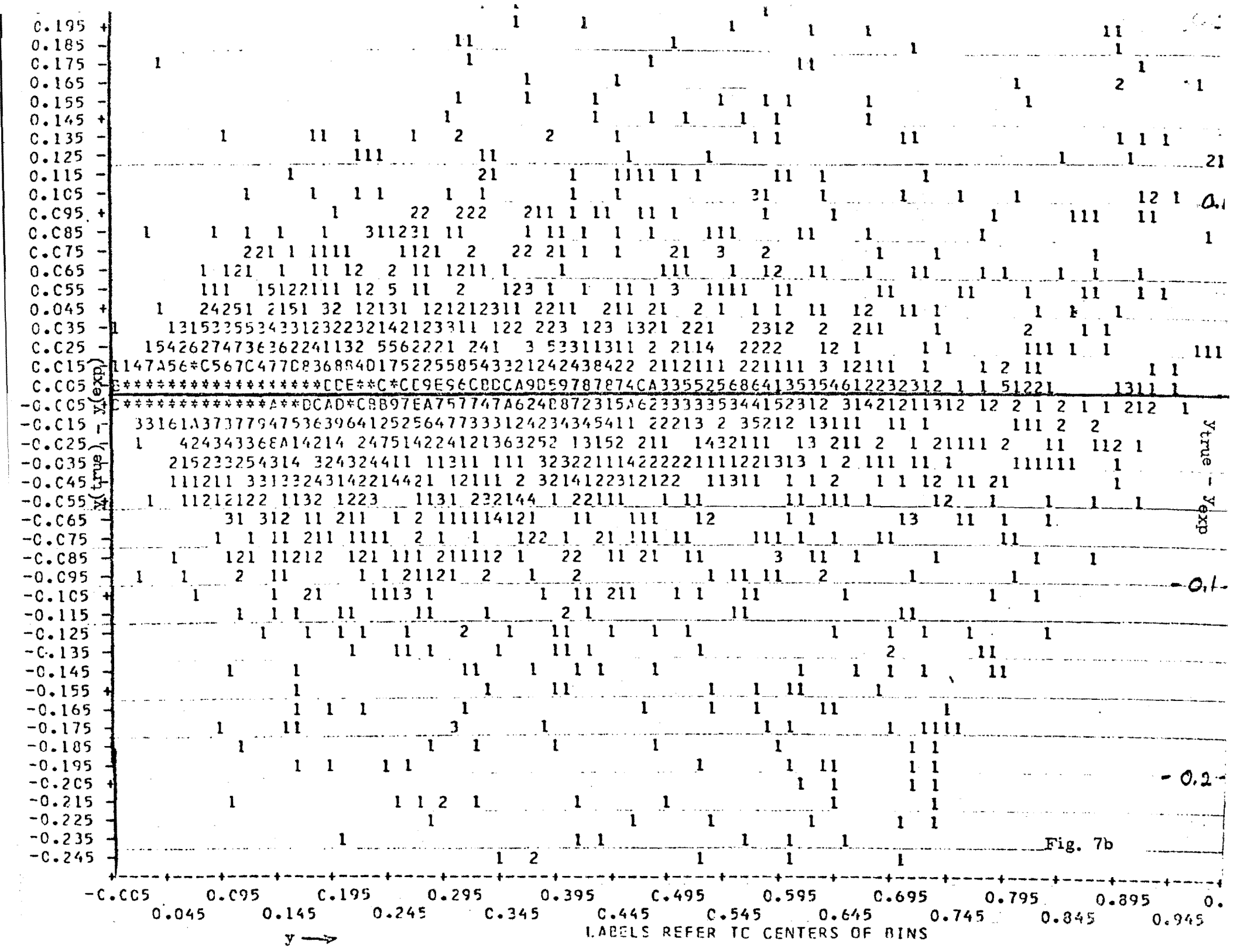
0.195
0.185
0.175
0.165
0.155
0.145
0.135
0.125
0.115
0.105
0.095
0.085
0.075
0.065
0.055
0.045
0.035
0.025
0.015
0.005
-0.005
-0.015
-0.025
-0.035
-0.045
-0.055
-0.065
-0.075
-0.085
-0.095
-0.105
-0.115
-0.125
-0.135
-0.145
-0.155
-0.165
-0.175
-0.185
-0.195
-0.205
-0.215
-0.225
-0.235
-0.245
y(true) - y(exp)
y_true - y_exp
0.1
-0.1
-0.2
-0.005
0.095
0.195
0.295
0.395
0.495
0.595
0.695
0.795
0.895
0.045
0.145
0.245
0.345
0.445
0.545
0.645
0.745
0.845
0.945
y ⟶
LABELS REFER TO CENTERS OF BINS

Fig. 7b

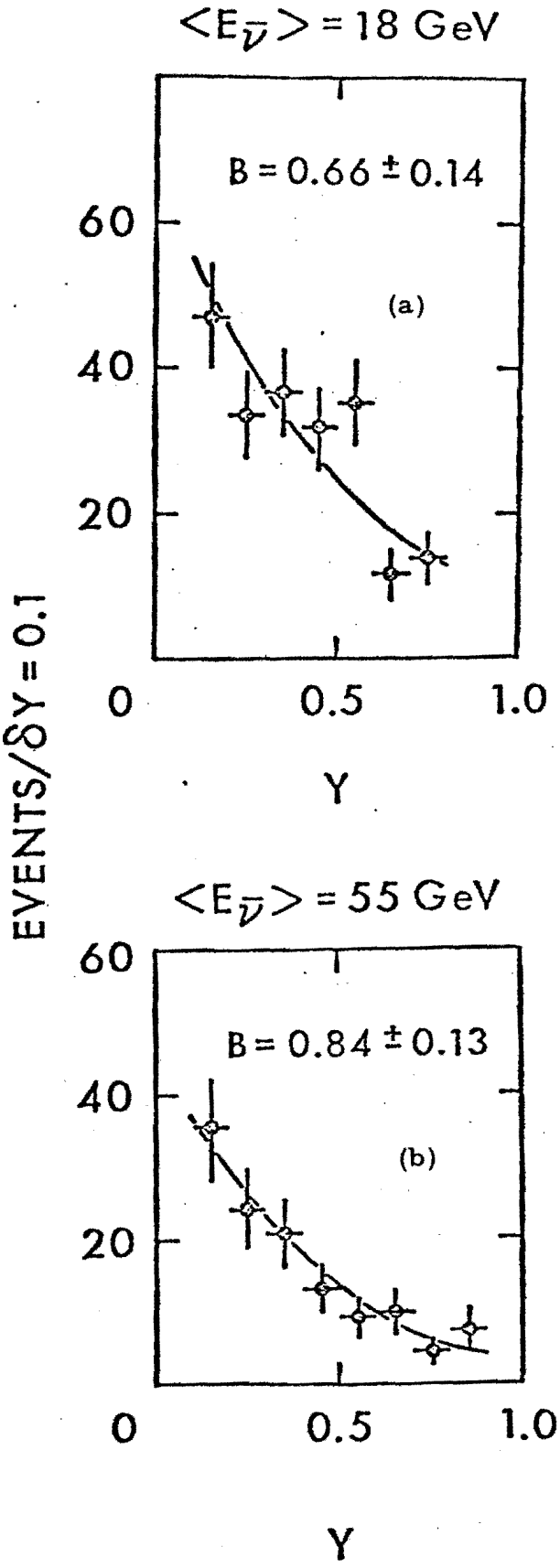
<E$_{\bar{\nu}}$> = 18 GeV
B = 0.66 ± 0.14
(a)
60
40
20
0
0.5
1.0
Y
EVENTS/δY = 0.1
<E$_{\bar{\nu}}$> = 55 GeV
B = 0.84 ± 0.13
(b)
60
40
20
0
0.5
1.0
Y

Fig. 8

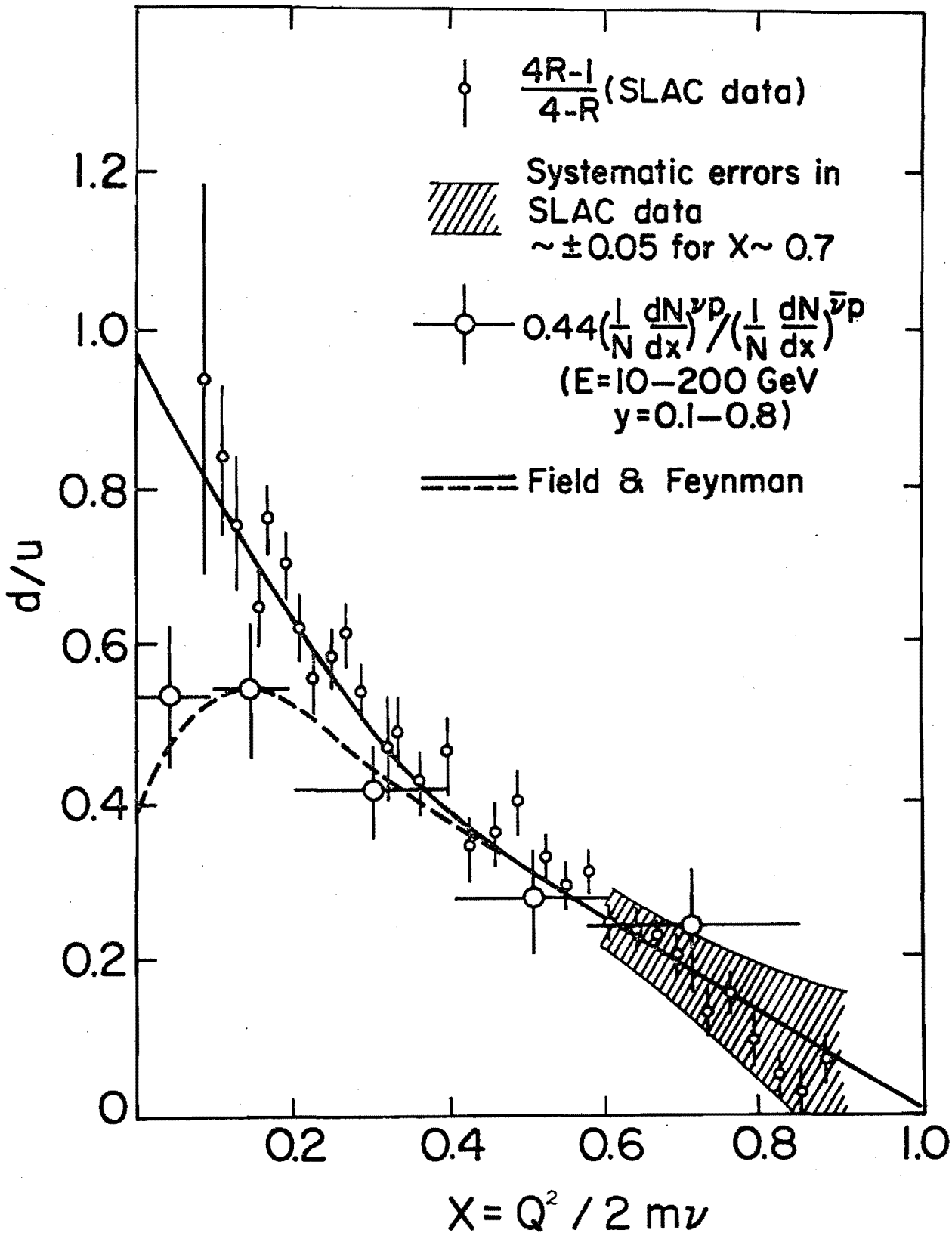
$\frac{4R-1}{4-R}$ (SLAC data)
Systematic errors in SLAC data
~±0.05 for X~ 0.7
$0.44(\frac{1}{N}\frac{dN}{dx})^{\nu p}/(\frac{1}{N}\frac{dN}{dx})^{\bar{\nu}p}$
(E=10–200 GeV
y=0.1–0.8)
Field & Feynman
d/u
X = Q² / 2 mν
0
0.2
0.4
0.6
0.8
1.0
1.2

Fig. 9

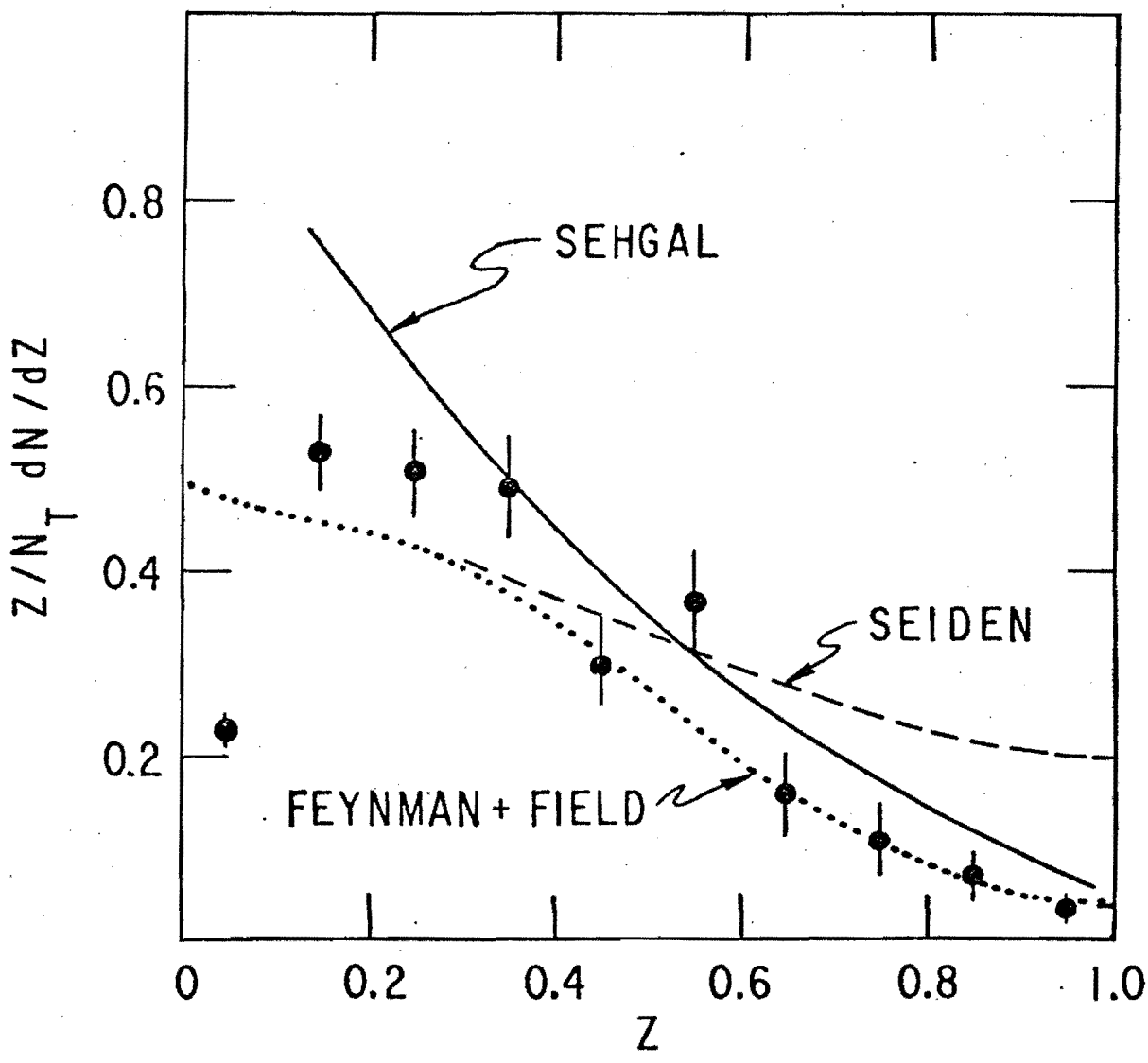
0.8
0.6
0.4
0.2
Z/N_T dN/dZ
SEHGAL
SEIDEN
FEYNMAN + FIELD
0
0.2
0.4
0.6
0.8
1.0
Z

Fig. 10

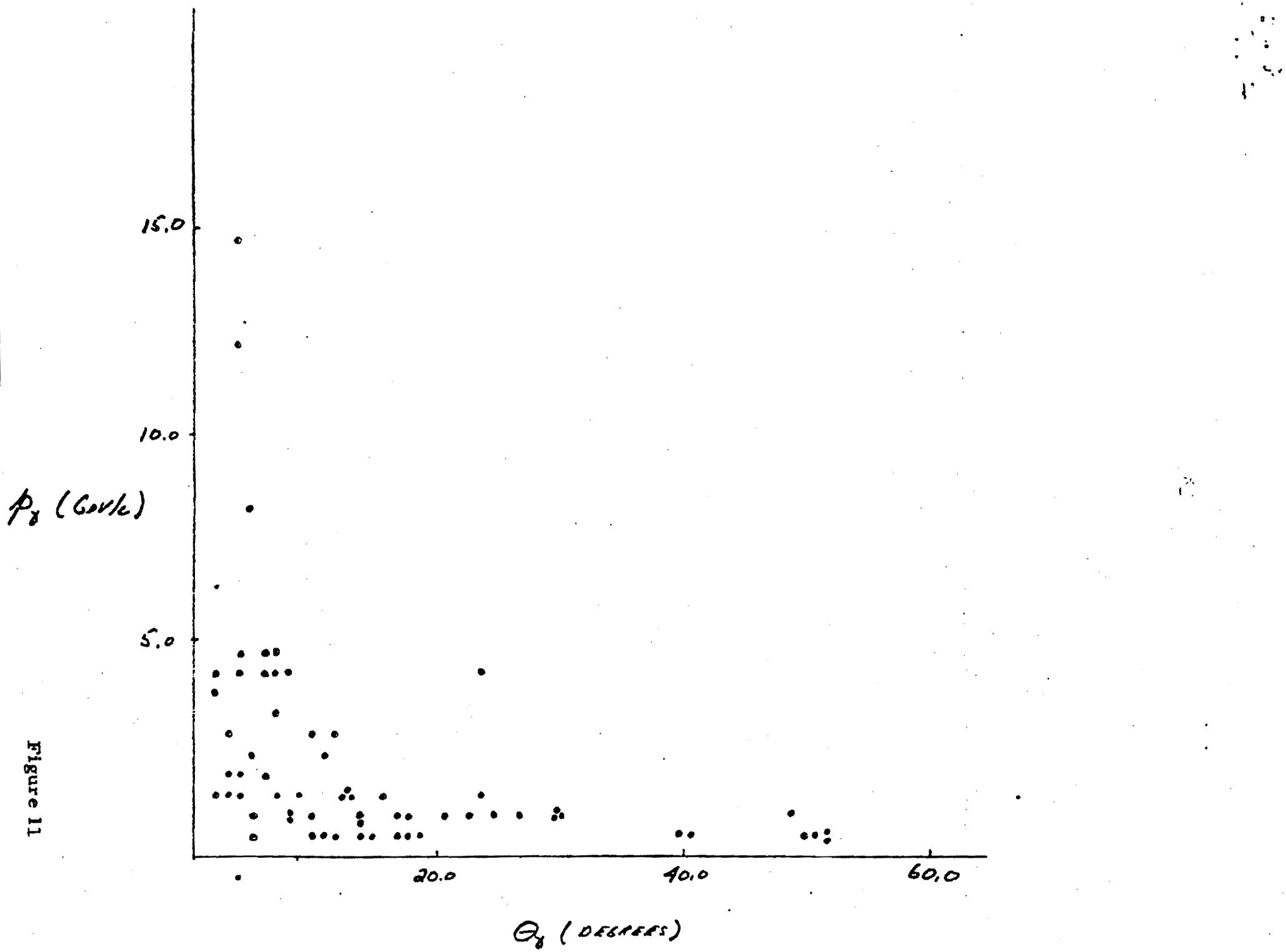

Figure 11

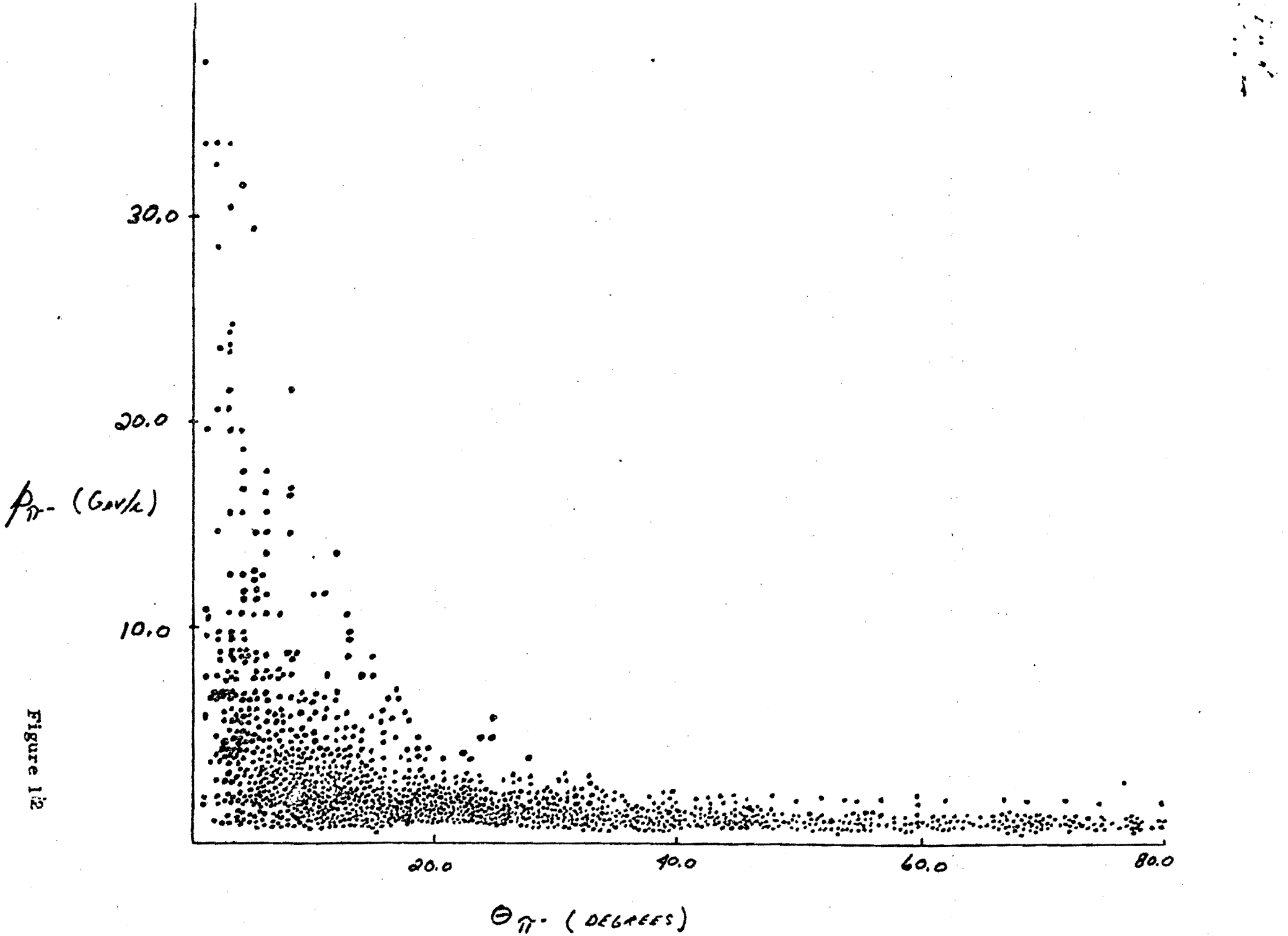

Figure 12

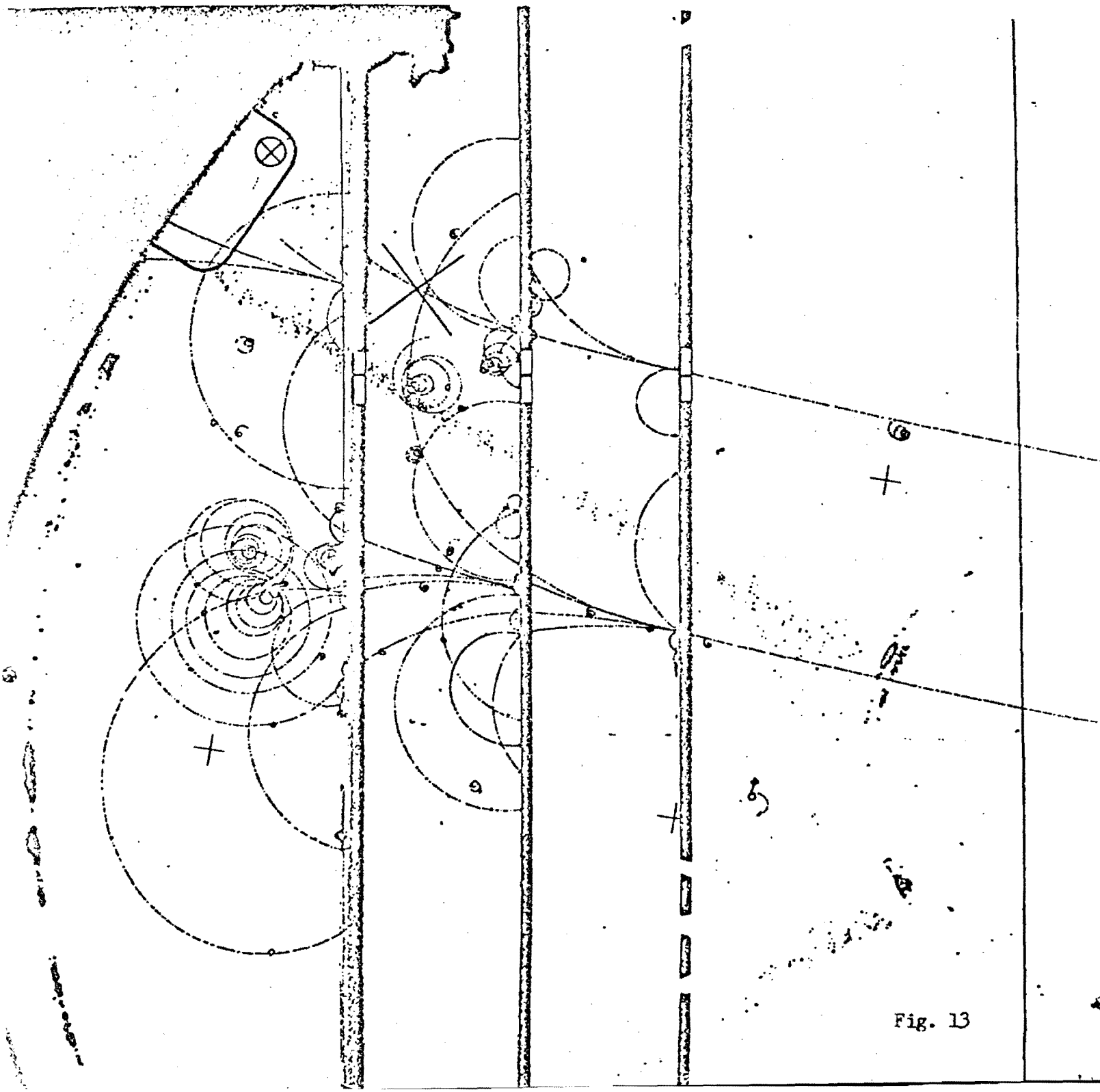

Fig. 13

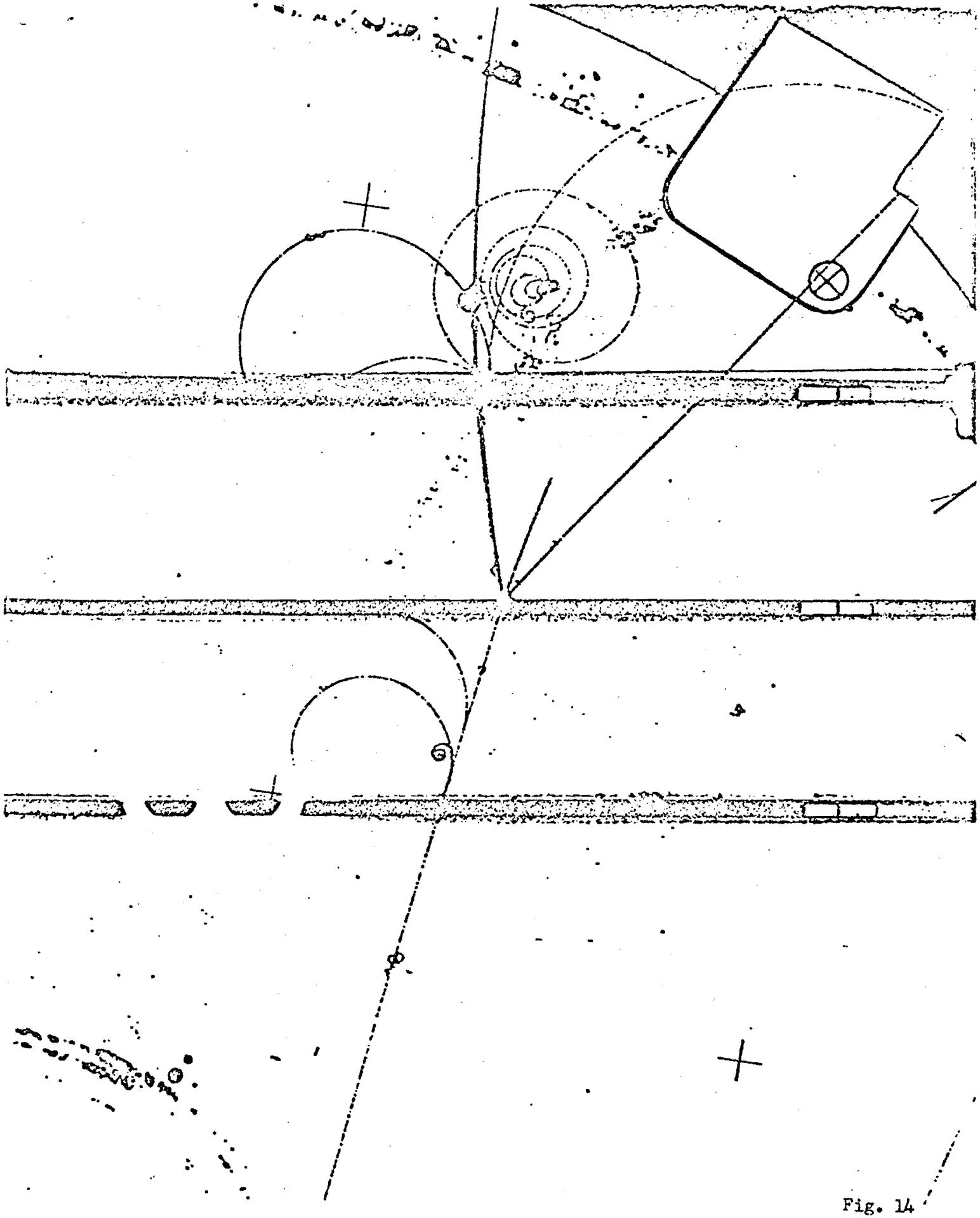

Fig. 14

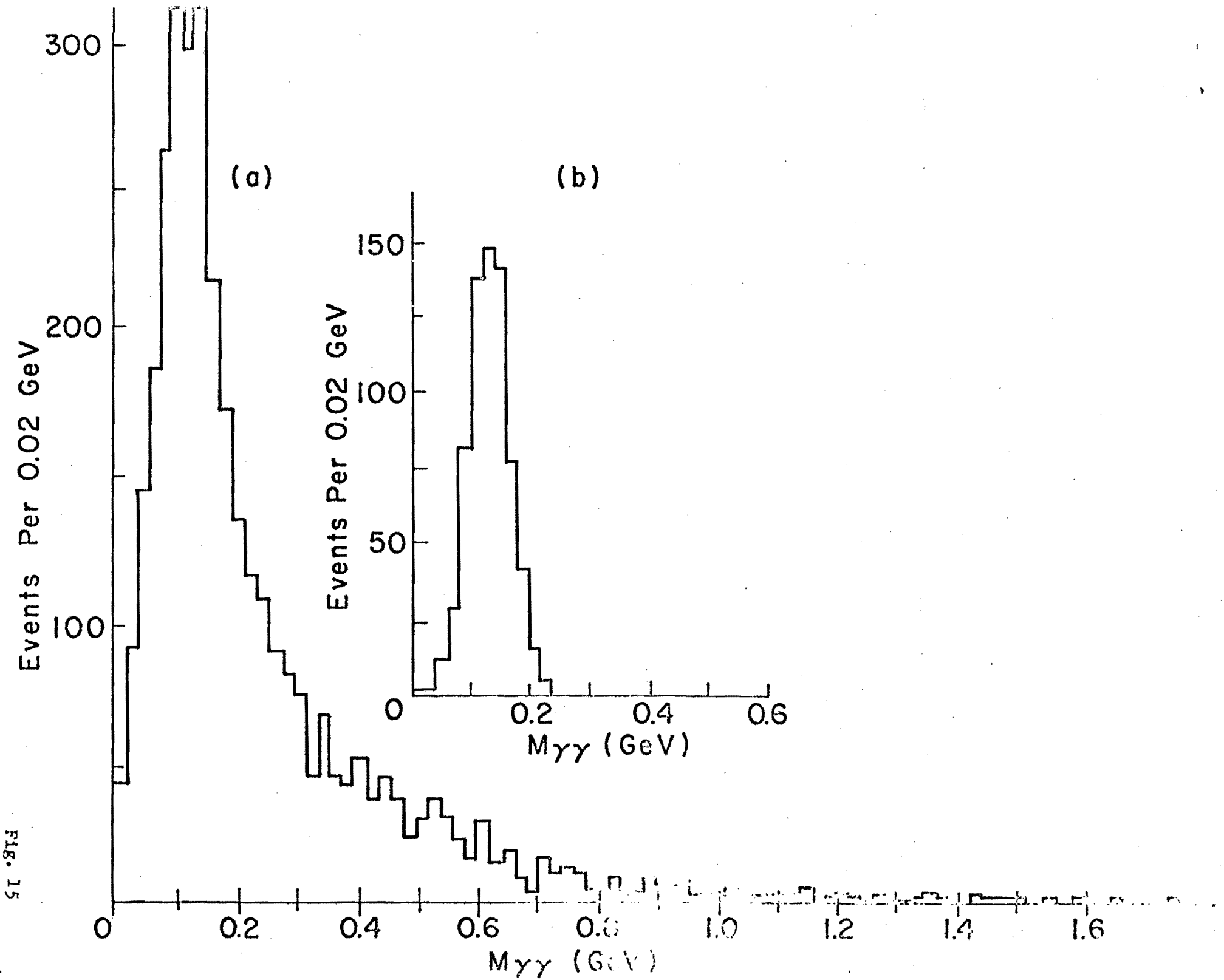
(a)
(b)
Events Per 0.02 GeV
Mγγ (GeV)
300
200
100
0
0.2
0.4
0.6
0.8
1.0
1.2
1.4
1.6
150
50

FIG. 15

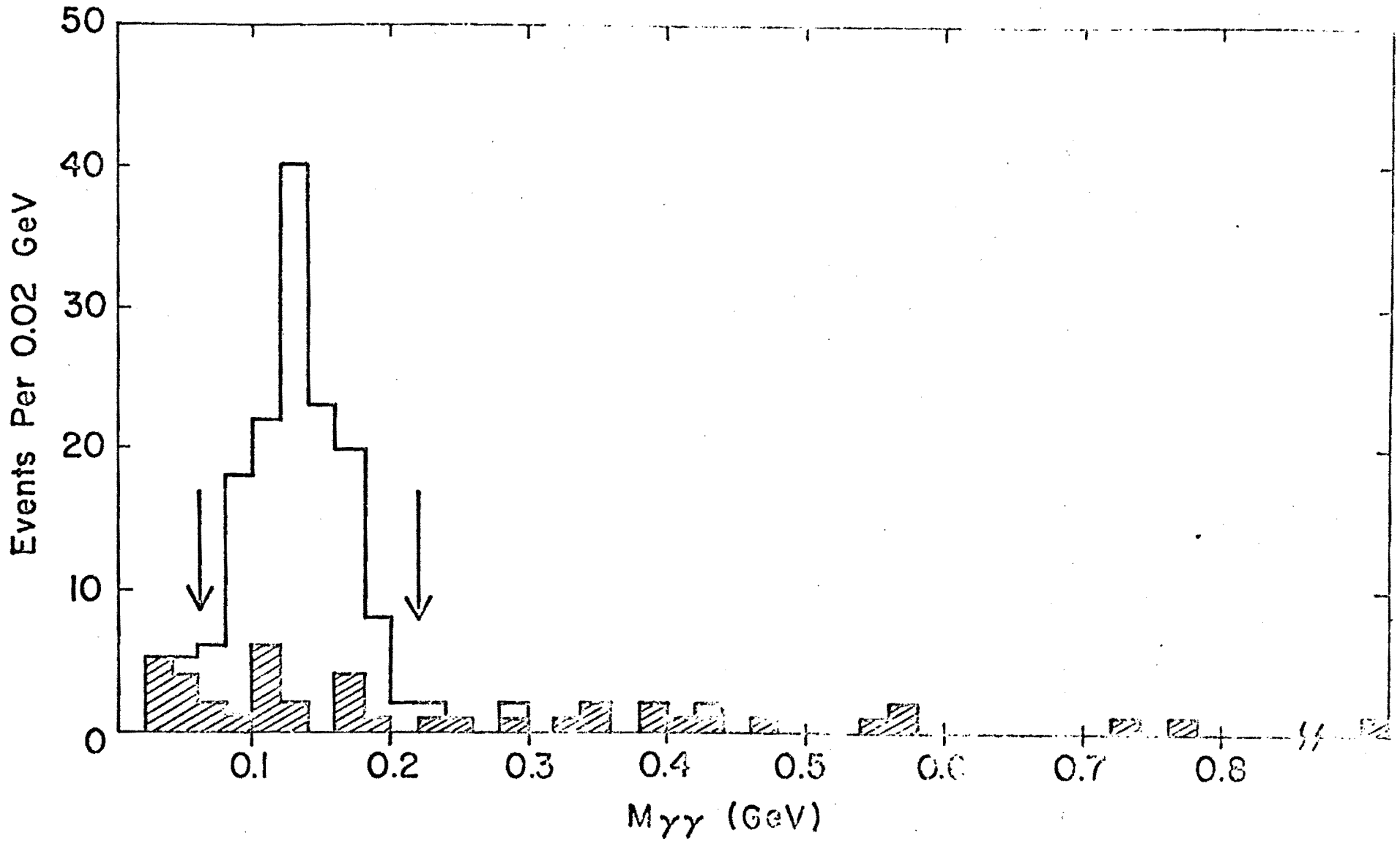

FIG. 16